

# Fine particle pH and gas-particle phase partitioning of inorganic species in Pasadena, California, during the 2010 CalNex campaign

Hongyu Guo<sup>1</sup>, Jiumeng Liu<sup>1,a</sup>, Karl D. Froyd<sup>2,3</sup>, James M. Roberts<sup>2</sup>, Patrick R. Veres<sup>2,3</sup>, Patrick L. Hayes<sup>3,4,5</sup>, Jose L. Jimenez<sup>3,5</sup>, Athanasios Nenes<sup>1,6,7,8</sup>, and Rodney J. Weber<sup>1</sup>

<sup>1</sup> School of Earth and Atmospheric Sciences, Georgia Institute of Technology, Atlanta, GA, USA

<sup>2</sup> Chemical Sciences Division, Earth System Research Laboratory, NOAA, Boulder, Colorado, USA

<sup>3</sup> Cooperative Institute for Research in Environmental Sciences (CIRES), Boulder, CO, USA

<sup>4</sup> Department of Chemistry, Université de Montréal, Montréal, Québec H3T 1J4, Canada

<sup>5</sup> Department of Chemistry and Biochemistry, University of Colorado Boulder, Boulder, CO, USA

<sup>6</sup> School of Chemical and Biomolecular Engineering, Georgia Institute of Technology, Atlanta, GA, USA

<sup>7</sup> Foundation for Research and Technology, Hellas, Greece

<sup>8</sup> National Observatory of Athens, Greece

<sup>a</sup> Now at Atmospheric Sciences and Global Change Division, Pacific Northwest National Laboratory, Richland, WA, USA

Correspondence to: Rodney J. Weber, ([rweber@eas.gatech.edu](mailto:rweber@eas.gatech.edu)), Athanasios Nenes ([athanasios.nenes@gatech.edu](mailto:athanasios.nenes@gatech.edu))

**Abstract.** pH is a fundamental aerosol property that affects ambient particle concentration and composition, linking pH to all aerosol environmental impacts. Here, PM<sub>1</sub> and PM<sub>2.5</sub> pH are calculated based on data from measurements during the California Research at the Nexus of Air Quality and Climate Change (CalNex) study from 15 May to 15 June 2010 in Pasadena CA. Particle pH and water were predicted with the ISORROPIA-II thermodynamic model and validated by comparing predicted to measured gas-particle partitioning of inorganic nitrate, ammonium and chloride. The study mean  $\pm$  standard deviation PM<sub>1</sub> pH was  $1.9 \pm 0.5$  for the SO<sub>4</sub><sup>2-</sup>-NO<sub>3</sub><sup>-</sup>-NH<sub>4</sub><sup>+</sup>-HNO<sub>3</sub>-NH<sub>3</sub> system. For PM<sub>2.5</sub>, internal mixing of sea salt components (SO<sub>4</sub><sup>2-</sup>-NO<sub>3</sub><sup>-</sup>-NH<sub>4</sub><sup>+</sup>-Na<sup>+</sup>-Cl<sup>-</sup>-K<sup>+</sup>-HNO<sub>3</sub>-NH<sub>3</sub>-HCl system) raised the bulk pH to  $2.7 \pm 0.3$  and improved predicted nitric acid partitioning with PM<sub>2.5</sub> components. The results show little effect of sea salt on PM<sub>1</sub> pH, but significant effects on PM<sub>2.5</sub> pH. A mean PM<sub>1</sub> pH of 1.9 at Pasadena was approximately one unit higher than what we have reported in the southeastern US, despite similar temperature, relative humidity and sulfate ranges and is due to higher total nitrate concentrations (nitric acid plus nitrate) relative to sulfate, a situation where particle water is affected by semi-volatile nitrate concentrations. Under these conditions nitric acid partitioning can further promote nitrate formation by increasing aerosol water, which raises pH by dilution, further increasing nitric acid partitioning and resulting in a significant increase in fine particle nitrate and pH. This study provides insights on the complex interactions between particle pH and nitrate in a summertime coastal environment and a contrast to recently reported pH in the eastern US in summer and winter and the eastern Mediterranean. All studies have consistently found highly acidic PM<sub>1</sub> with pH generally below 3.

## 1. Introduction

Ambient aerosol particles affect human health and climate (Lim et al., 2012; IPCC, 2013), and have many other environmental effects. Particle pH is linked to all of these by altering the fundamental aerosol properties of particle mass and chemical composition. For example, some important pathways leading to secondary organic aerosol (SOA) formation from biogenic volatile organic compounds (VOCs), such as isoprene and  $\alpha$ -pinene, are catalyzed by  $H^+$  (Jang et al., 2002; Gao et al., 2004; Edney et al., 2005; Surratt et al., 2007; Eddingsaas et al., 2010; Surratt et al., 2010; Han et al., 2016). pH directly affects particle mass and composition through altering the partitioning of both semi-volatile inorganic and organic acids between particle and gas phases (Guo et al., 2016). pH affects the nitrogen cycle through gas-particle partitioning of  $HNO_3$ - $NO_3^-$ ,  $NH_3$ - $NH_4^+$ , impacting deposition patterns due to large differences in gas versus particle dry deposition rates (Huebert and Robert, 1985; Duyzer, 1994; Schrader and Brummer, 2014).

Particle pH is linked to adverse health impacts, both directly and indirectly. Synergistic adverse health effects have been observed between ozone and acidic aerosols (Last, 1991; Enami et al., 2008) and epidemiological studies have reported adverse health outcomes associated with strong aerosol acidity (Koutrakis et al., 1988; Thurston et al., 1994; Dockery et al., 1996; Raizenne et al., 1996; Gwynn et al., 2000; Lelieveld et al., 2015). Low pH increases the solubility of transition metals, such as iron and copper (Meskhidze et al., 2003; Oakes et al., 2012; Longo et al., 2016; Fang et al., 2017), which have been linked to aerosol toxicity through aerosol oxidative effects (Ghio et al., 2012; Verma et al., 2014; Fang et al., 2015; Fang et al., 2017; Li et al., In press). Metal mobility also affects nutrient distributions with important impacts on photosynthesis productivity (Duce and Tindale, 1991; Meskhidze et al., 2003; Nenes et al., 2011; Ito and Xu, 2014; Myriokefalitakis et al., 2015), carbon sequestration and ocean oxygen levels (Ito et al., 2016).

Due to limitations with direct particle pH measurement techniques, fine particle pH has often been indirectly inferred from aerosol composition based on ion balances or cation-anion molar balances, e.g., ammonium to sulfate ( $NH_4^+/SO_4^{2-}$ ) molar ratios. However, these are largely inaccurate pH proxies (Guo et al., 2015; Hennigan et al., 2015; Guo et al., 2016; Weber et al., 2016), which if used can provide misleading indications on the level of acidity present in the aerosol and pH-related properties. Alternatively, particle pH is more accurately calculated with a thermodynamic model, such as ISORROPIA-II (Nenes et al., 1998; Fountoukis and Nenes, 2007) or E-AIM (Clegg et al., 1998; Wexler and Clegg, 2002; Clegg et al., 2003), which consider particle water, solution non-ideality, and variable dissociation of inorganic species in solution and equilibrium of semi-volatiles between gas and aerosol (aqueous and solid) phases. In “forward mode”, which utilizes both gas- and particle-phases inputs, the accuracy of pH predictions can be assessed by comparing predicted to measured partitioning of semi-volatile species, such as  $NH_3$ - $NH_4^+$ ,  $HNO_3$ - $NO_3^-$  and  $HCl$ - $Cl^-$  pairs. The semi-volatile species with the most information content about pH depend on the conditions at a specific location (e.g., when the specific component is not completely in the gas- or particle-phase).

This work adds to our investigation of particle pH in differing locations and under different emission characteristics. We have reported that ground level pH in the southeastern US is  $0.9 \pm 0.6$  (mean  $\pm$  standard deviation (SD)) in summer and  $2.0 \pm$

1.0 in winter (Guo et al., 2015), and  $0.8 \pm 1.0$  in the boundary layer and lower free troposphere ( $< 5$  km altitude) over broad regions of the eastern US in winter, based on aircraft data (Guo et al., 2016). A pH of  $1.3 \pm 1.1$  has also been reported in various air masses advected to Crete in the eastern Mediterranean (Bougiatioti et al., 2016b). This study focuses on particle pH in an urban coastal site, Pasadena, CA, and investigates the reasons for significantly higher nitrate mass loadings compared to those of the southeastern US (Zhang et al., 2007; Hand et al., 2012).

## 2. Methods

### 2.1 Sampling site

Aerosol and gas measurements were conducted on the California Institute of Technology campus in Pasadena, California (34.140582 N, 118.122455 W, altitude above sea level: 235 m), as part of the 2010 California Research at the Nexus of Air Quality and Climate Change (CalNex) campaign from 15 May to 15 June 2010 (Ryerson et al., 2013). The CalNex ground site was located within the Los Angeles Basin and approximately 16 km northeast of the central Los Angeles city (hereafter referred to as LA), and 5 km south of the San Gabriel Mountains. With the dominant wind from the southwest, the site was regularly impacted by emissions transported from the coast and central LA area (Washenfeller et al., 2011; Hayes et al., 2013). Meteorological data used in the following analysis is from the National Oceanic and Atmospheric Administrations (NOAA) CalNex researchers meteorological station.

### 2.2 Instrumentation

#### 2.2.1 Particles

**PILS-IC:** PM<sub>2.5</sub> (particles with aerodynamic diameters  $< 2.5$   $\mu\text{m}$  at ambient conditions) water-soluble ions were measured with a Particle-Into-Liquid Sampler coupled with Ion Chromatographs (PILS-IC), similar to that described elsewhere (Orsini et al., 2003; Hennigan et al., 2006; Sullivan et al., 2006; Peltier et al., 2007). The operation of PILS-IC during CalNex has been discussed by Liu et al. (2012) in detail. Ambient air was sampled through a URG (Chapel Hill, NC, USA) PM<sub>2.5</sub> cyclone and mixed with near 100°C water vapor generated from deionized water. After growth, droplets were collected by impaction, producing a continuous liquid sample for online IC analysis. All ambient data were blank-corrected by periodically measuring filtered ambient air. PM<sub>2.5</sub> anion data were available throughout the CalNex study, whereas cation data were only available for the last week (08-14 June). Since particle acidity predictions require both anion and cation data, discussions on PM<sub>2.5</sub> pH will include only the last week of data. The measurement uncertainties of anions and cations, based on calibration variability, sample air flow rates, liquid flow rates, and field blanks, were estimated to be 13% for anions and 8% for cations. Detection limits were 0.015  $\mu\text{g m}^{-3}$  SO<sub>4</sub><sup>2-</sup>, 0.03  $\mu\text{g m}^{-3}$  NO<sub>3</sub><sup>-</sup>, 0.01  $\mu\text{g m}^{-3}$  Cl<sup>-</sup> for anions, and 0.02  $\mu\text{g m}^{-3}$  NH<sub>4</sub><sup>+</sup>, 0.02  $\mu\text{g m}^{-3}$  Na<sup>+</sup>, 0.04  $\mu\text{g m}^{-3}$  K<sup>+</sup> for cations (Ca<sup>2+</sup> and Mg<sup>2+</sup> were not measured).

**AMS:** PM<sub>1</sub> non-refractory inorganic and organic components were measured by a high resolution time of flight aerosol mass spectrometer (HR-ToF-AMS, Aerodyne Research Inc., hereafter referred to as “AMS”; DeCarlo et al. (2006)). The operation procedure of the AMS during this study has been described in Hayes et al. (2013) and measurement uncertainty estimated at 30% (Middlebrook et al., 2012). The AMS detects non-refractory species in dried aerosols through an aerodynamic focusing lens, a detection chamber where aerosols are flash vaporized and ionized, followed by time-of-flight mass spectrometry. The comparison of AMS PM<sub>1</sub> and PILS-IC PM<sub>2.5</sub> measurements was summarized in Hayes et al. (2013) and is discussed further below. In the following analysis PM<sub>1</sub> species are AMS data and PM<sub>2.5</sub> species are PILS-IC data.

**PALMS:** Single aerosol composition and size for diameters 0.15-3  $\mu\text{m}$  were measured by an online Particle Analysis by Laser Mass Spectrometry (PALMS) (Murphy et al., 2006; Froyd et al., 2010). In this method, individual aerosols scatter light from a continuous laser beam and trigger an excimer laser that ionize the single particle. The resulting ions are analyzed by a time of flight mass spectrometer to generate a complete positive or negative mass spectrum per particle. In this study, PALMS data provides insights into the aerosol mixing state.

### 2.2.2 Gases

**QC-TILDAS:** gas-phase NH<sub>3</sub> was quantified using a Quantum Cascade Tunable Infrared Laser Differential Absorption Spectrometer (QC-TILDAS), developed by Aerodyne Research Inc. and described in details in Ellis et al. (2010). QC-TILDAS uses a thermoelectrically cooled pulsed Quantum Cascade (QC) laser, which measures NH<sub>3</sub> at 967 cm<sup>-1</sup> in the infrared regime. The laser beam is directed into an astigmatic Herriot absorption cell, where it passes between two highly reflective mirrors before leaving the cell and arriving at a thermoelectrically cooled Mercury Cadmium Telluride (HgCdTe) infrared detector. A 12 m heated (40  $\pm$  2°C) and insulated 3/8 inch perfluoroalkoxy (PFA) line (Clayborn Lab, Truckee, CA, USA) connects a short (10 cm; 8 m above ground) custom-designed quartz inlet to the QC-TILDAS. The inlet includes two ports for the introduction of calibration and background gas designed so that the flows follow the same path through the inlet as the ambient sample. Zero air measurements and ammonia calibrations were performed periodically during the CalNex campaign. The detection limit was 1.5 ppbv for 1 sec data and decreased to 0.42 ppbv for 1 min averaging data. The overall NH<sub>3</sub> measurement uncertainty was 10%.

**NI-PT-CIMS:** gas-phase HNO<sub>3</sub> and HCl measurements were made using a negative-ion proton-transfer chemical ionization mass spectrometer (NI-PT-CIMS; hereafter referred to as “CIMS”). Details of the NI-PT-CIMS design and operation during CalNex have been reported in Veres et al. (2008). Acidic molecules are ionized by proton transfer with acetate ions and detected as conjugate anions with a quadrupole mass spectrometer. The CIMS was placed on top of an instrument trailer at 3 m height with a heated (75°C) 1/8 inch Teflon inlet, 1.3 m in length, sampling at 5 m relative to ground level. (Possible biases in measured HNO<sub>3</sub> and HCl due to aerosol volatilization in the heated inlet is discussed in section 4.1). In the field, instrument backgrounds were quantified every 190 min for a duration of 30 min. The detection limits were 0.080 ppbv for HNO<sub>3</sub> and 0.055 ppbv for HCl. Overall measurement uncertainty was 35%. All gas-phase concentrations reported in ppbv

were converted to  $\mu\text{g m}^{-3}$  at ambient conditions to be consistent with particle-phase measurements and for thermodynamic calculations. In all cases, gas and particle concentrations are reported and utilized in the model using ambient conditions (i.e., all volumetric concentrations are at ambient temperature and pressure).

### 2.3 pH and gas-particle partitioning modeling

- 5 pH is defined as the negative logarithm of the hydronium ion ( $\text{H}_3\text{O}^+$ ) activity in an aqueous solution. Hereafter we denote  $\text{H}_3\text{O}^+$  as  $\text{H}^+$  for simplicity, while recognizing that the unhydrated hydrogen ion is rare in aqueous solutions. pH is given by,

$$pH = -\log_{10} \gamma_{\text{H}^+} H_{aq}^+ = -\log_{10} \frac{1000 \gamma_{\text{H}^+} H_{air}^+}{W_i + W_o} \cong -\log_{10} \frac{1000 \gamma_{\text{H}^+} H_{air}^+}{W_i} \quad (1)$$

- where  $\gamma_{\text{H}^+}$  is the hydronium ion activity coefficient (in this case assumed = 1),  $H_{aq}^+$  (mole  $\text{L}^{-1}$ ) the hydronium ion concentration in particle liquid water,  $H_{air}^+$  ( $\mu\text{g m}^{-3}$ ) the hydronium ion concentration per volume of air, and  $W_i$  and  $W_o$  ( $\mu\text{g m}^{-3}$ ) the bulk particle water concentrations associated with inorganic and organic species, respectively.  $W_o$  can be calculated  
 10 by Equation (5) in Guo et al. (2015). Both  $H_{air}^+$  and  $W_i$  are outputs of the thermodynamic model, ISORROPIA-II, which was used to determine the composition and phase state of an  $\text{NH}_4^+$ - $\text{SO}_4^{2-}$ - $\text{NO}_3^-$ -water inorganic aerosol in thermodynamic equilibrium with its corresponding gases. (In some cases  $\text{Cl}^-$ - $\text{Na}^+$ - $\text{K}^+$  were also included). A similar approach has been used in several studies for contrasting summer and winter conditions in the eastern US (Guo et al., 2015; Guo et al., 2016; Weber et al., 2016) and eastern Mediterranean (Bougiatioti et al., 2016a; Bougiatioti et al., 2016b).  
 15 In previous studies, the effect of  $W_o$  on pH has been investigated and found to be minor (Guo et al., 2015). pH in that study based solely on  $W_i$  was 0.15-0.23 units systematically lower than pH predicted with total particle water ( $W_i + W_o$ ) and highly correlated ( $R^2 = 0.97$ ). In this study,  $\Delta\text{pH}$  of +0.12 and +0.19 units were estimated when including  $W_o$  based on average and maximum organic hygroscopic parameter  $\kappa_{org}$  of 0.13 and 0.23, respectively (Mei et al., 2013). Sensitivity of pH to effects of  $W_o$  are smaller in CalNex due to smaller fractions of  $W_o$  to total particle water (21%) compared to that found in SOAS  
 20 (35%) (Southern Oxidant and Aerosol Study). Given this relatively small deviation (on average 0.12 unit), we report pH only considering  $W_i$ .

- ISORROPIA-II was run assuming particles were “metastable” with no solid precipitates ( $\text{H}^+$  is not stable in an effloresced aerosol); a reasonable assumption considering the high RH range observed during this study (mean  $\pm$  SD of RH =  $79 \pm 17\%$ ). In our previous pH studies, we only considered data for RH between 20-95%. At low RH (e.g.,  $< 20\%$ ), aerosols are  
 25 less likely to be in a completely liquid state (Ansari and Pandis, 2000; Malm and Day, 2001; Fountoukis and Nenes, 2007; Bertram et al., 2011), and the “glassy” SOA may impede the partitioning of semi-volatile species due to decreased diffusion in the particles (Ye et al., 2016), and uncertainties in predicted pH are expected to be large due to uncertain activity coefficients associated with highly concentrated solutions (Fountoukis et al., 2009). At RH  $> 95\%$ , large pH uncertainty is introduced due to the exponential growth in particle liquid water with RH and propagation of RH sensor uncertainties (Malm

and Day, 2001; Guo et al., 2015). The CalNex RH ranged from 22% to 100%, therefore periods for RH above 95% were excluded.

The model was also run in “forward” mode, which calculates the gas-particle equilibrium partitioning concentrations based on the input of total concentration of a species (i.e., gas + particle). Use of total species as ISORROPIA-II inputs produces substantially better predictions compared with only particle-phase concentration inputs in either “forward” or “reverse” modes since in the former cases (“forward” mode with only particle-phase input), particle-phase semi-volatile species concentration is under-predicted due to some fraction repartitioned into the gas-phase in the model, and in the latter cases (“reverse” mode), measurement errors often result in large model biases in pH (Hennigan et al., 2015).

The predicted gas- or particle-phase semi-volatile compounds can be compared to measurements for validating the thermodynamic calculations. Possible partitioning pairs for ISORROPIA-II are  $\text{HNO}_3\text{-NO}_3^-$ ,  $\text{NH}_3\text{-NH}_4^+$ , and  $\text{HCl-Cl}^-$  (discussed in Section 3.2&3.3). This method is effective when gas- and particle-phase components have substantial fractions in both the gas and particle phases. For example, in the southeastern US in summer, ammonia partitioning (gas/(gas+particle)) varied between 10 to 80%, whereas nitric acid partitioning was mostly near 80% and  $\text{PM}_{10}$  nitrate level close to the detection limit (larger uncertainty), making ammonia partitioning much more useful than nitric acid for evaluating thermodynamic models (Guo et al., 2015). In contrast, nitric acid partitioning, ranged from 0% to 100% (average ~ 50%) and so was used to evaluate pH predicted in the northeastern US in the cold season (Guo et al., 2016).

Using gas-particle phase partitioning to constrain particle pH can be complicated by the presence of multiple phases within the particle, which may distribute inorganic species amongst multiple phases, each with their own water activity and hence inorganic concentration. Lab studies show that liquid-liquid phase separations are always observed at O:C (organic aerosol atomic O to C ratio)  $\leq 0.5$ , whereas no phase separations occur for  $\text{O:C} \geq 0.8$  (Bertram et al., 2011; Song et al., 2012; You et al., 2013; You et al., 2014). The likelihood for phase separation decreases at higher RH ( $0.5 < \text{O:C} < 0.8$ ) and only has a weak dependence on T (Schill and Tolbert, 2013; You and Bertram, 2015). For conditions during SOAS ( $\text{O:C} = 0.75 \pm 0.12$ ,  $\text{RH} = 74 \pm 16\%$ ,  $T = 25 \pm 3^\circ\text{C}$ ), we found that thermodynamic calculations accurately predicted bulk particle water and ammonia partitioning over the complete T (18 to  $33^\circ\text{C}$ ) and RH (36 to 96%) ranges (Guo et al., 2015). During the Wintertime Investigation of Transport, Emissions, and Reactivity (WINTER) aircraft study ( $\text{O:C} = 0.78 \pm 0.11$ ,  $T = 0 \pm 8^\circ\text{C}$ ), we found that  $\text{HNO}_3\text{-NO}_3^-$  partitioning was accurately predicted for  $\text{RH} > 60\%$  (Guo et al., 2016). Compared to SOAS and WINTER (both in the eastern US), in this study the smaller O:C ( $0.52 \pm 0.10$ ) (Hayes et al., 2015) mean we cannot outright exclude the possibility of phase separation, but very high RH ( $79 \pm 17\%$ ) makes it less likely.

In running ISORROPIA-II to predict pH and semi-volatile species partitioning, it is also assumed that the particles are internally mixed, that pH does not vary with particle size (i.e., bulk properties represent the overall aerosol pH), and that the ambient aerosols and gases are in thermodynamic equilibrium. For the WINTER study, which included measurements over coastal and marine areas, we found that  $\text{PM}_{10}$  pH was accurately predicted with only particle-phase  $\text{SO}_4^{2-}$ ,  $\text{NO}_3^-$ ,  $\text{NH}_4^+$  (and gas-phase  $\text{HNO}_3$ ); whereas sea salt components had some, but generally small, effects on the prediction of particle pH (except on rare occasions when the mole fraction of NaCl to total soluble inorganic ions was greater than 50%) (Guo et al.,

2016). The mixing state of sea salts with  $\text{SO}_4^{2-}$ ,  $\text{NO}_3^-$ ,  $\text{NH}_4^+$  is a critical issue in predicting particle pH in LA and is discussed below.

### 3. Results

#### 3.1 $\text{PM}_1$ and $\text{PM}_{2.5}$ inorganic composition and gas-particle partitioning

5 Time series for various measured parameters during CalNex are shown in Figure 1. CalNex T and RH were  $18 \pm 4^\circ\text{C}$  and  $79 \pm 17\%$  (mean  $\pm$  SD). During the first half of the campaign, 15 May to 29 May, daily maximum T was below  $26^\circ\text{C}$  and  $\text{PM}_1$  (AMS) and  $\text{PM}_{2.5}$  (PILS-IC)  $\text{SO}_4^{2-}$ ,  $\text{NO}_3^-$ ,  $\text{NH}_4^+$  showed a general decreasing trend ( $\text{PM}_{2.5}$   $\text{NH}_4^+$  data was not available in this period). The second half of the campaign started with a warmer period (30 May to 7 June), with the highest T reaching  $29^\circ\text{C}$ . During this period,  $\text{SO}_4^{2-}$ ,  $\text{NO}_3^-$ ,  $\text{NH}_4^+$ , and  $\text{HNO}_3$  were significantly higher than the first half and reached campaign  
10 maximums of  $9.7 \mu\text{g m}^{-3}$   $\text{PM}_1$   $\text{SO}_4^{2-}$ ,  $20.1 \mu\text{g m}^{-3}$   $\text{PM}_1$   $\text{NO}_3^-$ ,  $9.6 \mu\text{g m}^{-3}$   $\text{PM}_1$   $\text{NH}_4^+$ , and  $33.1 \mu\text{g m}^{-3}$   $\text{HNO}_3$ . The peak concentrations of combined  $\text{PM}_1$  inorganics alone exceeded The National Ambient Air Quality Standard (NAAQS)  $\text{PM}_{2.5}$  24-hour limit of  $35 \mu\text{g m}^{-3}$  (<https://www.epa.gov/criteria-air-pollutants/naaqs-table>), with the largest contribution from  $\text{NO}_3^-$ . Gaseous components other than  $\text{HNO}_3$ , such as  $\text{NH}_3$  and  $\text{HCl}$ , showed different patterns than the above species, indicating different sources and sinks.

15  $\text{PM}_1$  (AMS)  $\text{SO}_4^{2-}$ ,  $\text{NO}_3^-$ ,  $\text{NH}_4^+$  were highly correlated with  $\text{PM}_{2.5}$  (PILS-IC) measurements, with  $R^2$  between 0.8 and 0.9 (Fig. S1).  $\text{PM}_1/\text{PM}_{2.5}$  mass ratios were  $97.5 \pm 5.4\%$  for  $\text{SO}_4^{2-}$ ,  $63.5 \pm 22.1\%$  for  $\text{NO}_3^-$ , and  $92.3 \pm 9.9\%$  for  $\text{NH}_4^+$ . Note that, the mass fractions for  $\text{SO}_4^{2-}$  and  $\text{NO}_3^-$  are campaign averages, but  $\text{NH}_4^+$  mass fraction is only for the last week when  $\text{PM}_{2.5}$   $\text{NH}_4^+$  was available. Nearly 40% of the  $\text{NO}_3^-$  was found between 1 and  $2.5 \mu\text{m}$ , whereas most  $\text{SO}_4^{2-}$  and  $\text{NH}_4^+$  were associated with  $\text{PM}_1$ . (Ratios based on regression slopes are shown in Fig. S1). Hence, the  $\text{NO}_3^-$  for the 1 to  $2.5 \mu\text{m}$  size  
20 range was likely associated with some non-volatile cations, such as  $\text{Na}^+$  and  $\text{K}^+$  instead of  $\text{NH}_4^+$ . The  $\text{PM}_{2.5}$   $\text{Cl}^-/\text{Na}^+$  molar ratio was  $0.5 \pm 0.2$ . Given that these species are mainly transported from the coastal regions in the form of sea salts ( $\text{NaCl}$ ), this indicates that roughly half of the  $\text{Na}^+$  had reacted with  $\text{HNO}_3$  resulting in depleted  $\text{Cl}^-$  (Robbins et al., 1959; Langer et al., 1997). These results are consistent with the analysis of Hayes et al. (2013).

Measurements of semi-volatile particle ( $\text{NO}_3^-$ ,  $\text{NH}_4^+$ ,  $\text{Cl}^-$ ) and corresponding inorganic gases, ( $\text{HNO}_3$ ,  $\text{NH}_3$ ,  $\text{HCl}$ ) are used to  
25 investigate partitioning. The gas-particle phase partitioning is described as the particle-phase mass concentration divided by the total mass concentration (gas + particle), e.g.,  $\epsilon(\text{NO}_3^-) = \text{NO}_3^-/(\text{HNO}_3 + \text{NO}_3^-)$ . The campaign average partitioning ratios were as follows; for  $\text{PM}_1$   $\epsilon(\text{NO}_3^-) = 39 \pm 16\%$ ,  $\text{PM}_1$   $\epsilon(\text{NH}_4^+) = 56 \pm 26\%$ ,  $\text{PM}_{2.5}$   $\epsilon(\text{NO}_3^-) = 54 \pm 10\%$ , and  $\text{PM}_{2.5}$   $\epsilon(\text{Cl}^-) = 39 \pm 26\%$ . All partitioning ratios are near 50%, making them useful for assessing pH predictions by comparing measured versus ISORROPIA-predicted ratios.

### 3.2 PM<sub>1</sub> pH prediction and verification

PM<sub>1</sub> pH was determined to be on average ( $\pm$  SD)  $1.9 \pm 0.5$  for the complete study, for model inputs of PM<sub>1</sub> inorganic AMS-measured components  $\text{SO}_4^{2-}$ ,  $\text{NO}_3^-$ ,  $\text{NH}_4^+$ , and gases  $\text{HNO}_3$  and  $\text{NH}_3$ . Although the CalNex ground site was influenced by sea salt components,  $\text{Na}^+$  and  $\text{Cl}^-$  were not included in the PM<sub>1</sub> pH since NaCl is typically found mainly at sizes above  $1\text{ }\mu\text{m}$  and the mixing states of PM<sub>1</sub> NaCl with  $\text{SO}_4^{2-}$ ,  $\text{NO}_3^-$ ,  $\text{NH}_4^+$  remains to be investigated. PALMS single particle data indicated that for the particle size range with  $D_{\text{ve}}$  (dry volume-equivalent diameter) between 0.15 and  $780\text{ nm}$  ( $\sim 1\text{ }\mu\text{m}$ ), by number 27% of PM<sub>1</sub> sea salt particles ( $\text{Na}^+$ -rich particles without crustal materials) had observable  $\text{NO}_3^-$  signals and by mass only 12% of PM<sub>1</sub> are sea salt types (Table 1), suggesting external mixing of NaCl with  $\text{NO}_3^-$  is the main form. For the 1 to  $2.5\text{ }\mu\text{m}$  size range the number and mass fractions were 85% and 63%, respectively.

We assess predicted pH from the thermodynamic model by comparing predicted and measured gas-particle partitioning of  $\text{NH}_3$ - $\text{NH}_4^+$ ,  $\text{HNO}_3$ - $\text{NO}_3^-$ . Comparison of  $\text{HNO}_3$ - $\text{NO}_3^-$  and  $\text{NH}_3$ - $\text{NH}_4^+$  predictions to their measured values is shown as Figure 2. Gas-phase  $\text{HNO}_3$ ,  $\text{NH}_3$  and particle-phase  $\text{NH}_4^+$  are on average within 10% and highly correlated,  $R^2 > 0.8$ . Despite a high correlation ( $R^2 = 0.76$ ), ISORROPIA-II predicted particle-phase  $\text{NO}_3^-$  is systematically higher than observed, with a regression slope of 1.28. Two bands are observed that are related to RH or time of day (Fig. 2b); for mid-range RH (50-70%) daytime data, ISORROPIA-II slightly under-predicts  $\text{NO}_3^-$  and for high RH ( $\sim 90\%$ ) nighttime data,  $\text{NO}_3^-$  is over-predicted. This leads to a regression slope of 2 comparing predicted to measured  $\epsilon(\text{NO}_3^-)$  and a large intercept (Fig. 2c, also see Fig. S5). In contrast, predicted versus measured  $\epsilon(\text{NH}_4^+)$  is close to 1:1 and highly correlated ( $R^2 = 0.8$ , Figure 2f), and there is a much weaker systematic variability related to RH or time of day.

### 3.3 PM<sub>2.5</sub> pH prediction and verification

Predicting the bulk pH of PM<sub>2.5</sub> is more complicated since the particles larger than  $1\text{ }\mu\text{m}$  in the PM<sub>2.5</sub> fraction are not necessarily in equilibrium due to increased timescale for equilibration ( $> 20\text{-}30\text{ mins}$ ) (Fountoukis et al., 2009), especially in an environment with rapidly changing concentrations of key species (e.g.  $\text{HNO}_3$ ). This leads to greater uncertainty when predicting partitioning of semi-volatile species. Furthermore, the pH analysis now needs to consider sea salt components ( $\text{SO}_4^{2-}$ - $\text{NO}_3^-$ - $\text{NH}_4^+$ - $\text{Na}^+$ - $\text{Cl}^-$ - $\text{K}^+$ - $\text{HNO}_3$ - $\text{NH}_3$ - $\text{HCl}$  system). Whereas single particle PALMS data suggested that only a small fraction (27%) of the sea salt particles less than  $1\text{ }\mu\text{m}$  were internally mixed with nitrate, for sizes between 1 and  $2.5\text{ }\mu\text{m}$ , the majority (85%) were. Overall we find bulk PM<sub>2.5</sub> pH considering sea salt components higher than PM<sub>1</sub> by 0.8 units on average. For data from the last week of the study (i.e., period of PILS data that includes measurements of sea-salt components), PM<sub>1</sub> pH was  $1.9 \pm 0.4$ , similar to that of the complete study ( $1.9 \pm 0.5$ ), and in contrast to an average PM<sub>2.5</sub> pH of  $2.7 \pm 0.3$ . A comparison of the pH is shown in Figure 3. Addition of non-volatile  $\text{Na}^+$  and  $\text{K}^+$  increases pH.  $\text{Na}^+$  is the more important cation in this case, as the  $\text{Na}^+$  levels were several times larger than  $\text{K}^+$  ( $0.77 \pm 0.39$  vs.  $0.20 \pm 0.09\text{ }\mu\text{g m}^{-3}$ , or  $0.33$  vs.  $0.05\text{ mol m}^{-3}$ ).



To examine the effects of sea salt components on the thermodynamic predictions, we compared the observed to measured partitioning of PM<sub>2.5</sub> semi-volatile species in Figure 4. ISORROPIA-II was run with two differing inputs, one with Na<sup>+</sup>, Cl<sup>-</sup>, K<sup>+</sup> and the other run without these ions. In both cases only PILS-IC PM<sub>2.5</sub> data are used. All other input parameters, including NH<sub>4</sub><sup>+</sup>, SO<sub>4</sub><sup>2-</sup>, NO<sub>3</sub><sup>-</sup>, RH, and T, were the same. Figure 4 shows that inclusion of Na<sup>+</sup>, Cl<sup>-</sup>, K<sup>+</sup> improves the prediction of HNO<sub>3</sub>-NO<sub>3</sub><sup>-</sup> partitioning. For HNO<sub>3</sub>, NO<sub>3</sub><sup>-</sup> and  $\epsilon(\text{NO}_3^-)$ , predicted levels are somewhat closer to the measurements and the scatter in the data is reduced. However, like the PM<sub>1</sub> analysis above, the slope between predicted and measured  $\epsilon(\text{NO}_3^-)$ , 2.4, is significantly larger than 1. The deviation is again related to RH, resulting from a diurnal dependence. Unlike the HNO<sub>3</sub>-NO<sub>3</sub><sup>-</sup> partitioning, NH<sub>3</sub>-NH<sub>4</sub><sup>+</sup> partitioning is not as sensitive to inclusion of Na<sup>+</sup>, Cl<sup>-</sup>, K<sup>+</sup>. Overall,  $\epsilon(\text{NH}_4^+)$  is on average underestimated by 17% compared to measured (average ratio). HCl-Cl<sup>-</sup> partitioning is well captured by ISORROPIA-II with regression slopes of 1.05, 0.95, 1.14 and R<sup>2</sup> of 0.98, 0.84, 0.81 for HCl, Cl<sup>-</sup>,  $\epsilon(\text{Cl}^-)$ , respectively.

An analytical calculation of HNO<sub>3</sub>-NO<sub>3</sub><sup>-</sup> partitioning can also be used to assess whether the shift of one pH unit caused by Na<sup>+</sup>, Cl<sup>-</sup>, K<sup>+</sup> is consistent with observed nitric acid partitioning for PM<sub>2.5</sub>. The analytical calculation is based on Equation 3 in Guo et al. (2016) and a detailed equation derivation can be found in supplemental material section 2. To minimize the effects of T and  $W_i$  variability on partitioning, and focus on the role of pH, data for a relatively small T (17-23°C) and  $W_i$  (5-15  $\mu\text{g m}^{-3}$ ) range were selected. Predicted activity coefficients,  $\gamma_{H^+}$  and  $\gamma_{\text{NO}_3^-}$ , extracted from ISORROPIA-II, were input in the analytical calculation to account for solution non-ideality. The product of the activity coefficients,  $\gamma_{H^+}\gamma_{\text{NO}_3^-}$ , was on average 0.28 with Na<sup>+</sup>, Cl<sup>-</sup>, K<sup>+</sup> in the model and 0.19 without Na<sup>+</sup>, Cl<sup>-</sup>, K<sup>+</sup> ( $\gamma_{H^+}\gamma_{\text{NO}_3^-}$  is smaller without Na<sup>+</sup>, Cl<sup>-</sup>, K<sup>+</sup> due to less predicted  $W_i$ , thus overall larger ionic strength). The analytical calculated S curves are plotted with the measurements and ISORROPIA-II predictions in Figure 5. As noted, including these components changes the activity coefficient  $\gamma_{H^+}\gamma_{\text{NO}_3^-}$  (as can be seen by the difference in the two curves in Figure 5) and also slightly increases the liquid water. But the most important effect is reducing H<sup>+</sup>, resulting in a shift to higher pH. This analysis also shows that the measured  $\epsilon(\text{NO}_3^-)$  comes into better agreement with its theoretical S curve for the SO<sub>4</sub><sup>2-</sup>-NO<sub>3</sub><sup>-</sup>-NH<sub>4</sub><sup>+</sup>-Na<sup>+</sup>-Cl<sup>-</sup>-K<sup>+</sup>-HNO<sub>3</sub>-NH<sub>3</sub>-HCl system (red points closer to red curve compared to blue points and blue curve). Similar to  $\epsilon(\text{NO}_3^-)$ , measured  $\epsilon(\text{Cl}^-)$  is also found to be in good agreement with S curve (Fig. S2).

### 3.4 Average diurnal trends

**PM<sub>1</sub>:** The diurnal variations of T, RH, pH, LWC, HNO<sub>3</sub>-NO<sub>3</sub><sup>-</sup> and NH<sub>3</sub>-NH<sub>4</sub><sup>+</sup> partitioning are shown together in Figure 6. Due to the inverse variation between T and RH diurnal patterns, predicted particle water ( $W_i$ ) reached a daily maximum before dawn and decreased rapidly with RH after sunrise. To be consistent with pH, particle water data is not plotted for RH above 95%. (For RH above 95%, particle water increased continuously at night until reaching the daily highest RH at 5:30). Between 13:00 and 20:00 local time,  $W_i$  stayed consistently low ( $\sim 5 \mu\text{g m}^{-3}$ ). PM<sub>1</sub> pH generally tracked liquid water. pH was lower in the daytime due to less liquid water, reaching a minimum value of 1.6 at approximately 16:00. After that, pH

continued to increase to its daily maximum of 2.4 at midnight, tracking the liquid water concentrations. This pH diurnal pattern is similar to that observed in the southeastern US (Guo et al., 2015). A very large peak in gaseous  $\text{HNO}_3$  was observed during the day produced from rapid photochemical reactions of  $\text{NO}_x$  with the hydroxyl radical in the LA outflows (Veres et al., 2011). In contrast,  $\text{NO}_3^-$  peaked at dawn under conditions of low T and high RH, which favored nitrate condensation (S curves shifted to lower pH, see Fig. S3 and S4), consistent with a previous study in Mexico City (Hennigan et al., 2008). There was also a small peak in  $\text{NO}_3^-$  near midday when  $\text{HNO}_3$  peaked, simply due to the large amount of fresh  $\text{HNO}_3$ , despite the trend of a continuous  $\varepsilon(\text{NO}_3^-)$  decrease. The diurnal variation of  $\varepsilon(\text{NO}_3^-)$  was similar to liquid water and pH. The  $\text{PM}_1$   $\text{NH}_4^+$  trend followed  $\text{NO}_3^-$  and all inorganic species ( $\text{NH}_4^+$ ,  $\text{SO}_4^{2-}$ ,  $\text{NO}_3^-$ ) exhibited a peak during the day.  $\varepsilon(\text{NH}_4^+)$  had a similar diurnal pattern as  $\varepsilon(\text{NO}_3^-)$ .

**PM<sub>2.5</sub>:** Figure 7 compares the diurnal trends of  $\text{PM}_1$  pH (AMS data,  $\text{SO}_4^{2-}$ ,  $\text{NO}_3^-$ ,  $\text{NH}_4^+$ ) and  $\text{PM}_{2.5}$  pH (PILS-IC  $\text{SO}_4^{2-}$ ,  $\text{NO}_3^-$ ,  $\text{NH}_4^+$ ,  $\text{Na}^+$ ,  $\text{Cl}^-$ ,  $\text{K}^+$ ) for the last week of the study.  $\text{PM}_1$  pH had a similar profile to that for the complete study; lower in the afternoon and followed the  $W_i$  trend, whereas the  $\text{PM}_{2.5}$  diurnal pH trend was nearly flat. The difference was caused by more non-volatile  $\text{Na}^+$  than volatile  $\text{Cl}^-$  ( $\text{PM}_{2.5}$   $\text{Cl}^-/\text{Na}^+$  molar ratio was  $0.5 \pm 0.2$ ), which is related to the  $\text{HNO}_3$  and  $\text{HCl}$  trends. Sea salt components in the 1 to 2.5  $\mu\text{m}$  size range react with the daytime high  $\text{HNO}_3$  forming  $\text{NO}_3^-$  and gas-phase  $\text{HCl}$  (simplified as  $\text{Cl}^- + \text{HNO}_3 \rightarrow \text{NO}_3^- + \text{HCl}$ ) (Robbins et al., 1959; Langer et al., 1997). This “chloride depletion” is a result of the higher volatility of  $\text{HCl}$  versus  $\text{HNO}_3$  in the deliquesced sea salt aerosol (Nenes et al., 1998; Fountoukis and Nenes, 2007). The process can partly account for the large  $\text{HCl}$  peak and stronger  $\text{Cl}^-$  depletion (wider gap between  $\text{Na}^+$  and  $\text{Cl}^-$ ) during the day, coinciding with high  $\text{HNO}_3$  and low  $W_i$  (evaporation of  $\text{HCl}$  occurs during evaporation of droplets). The slightly higher  $\text{Na}^+$  generally increased pH due to the added non-volatile cations. These data are consistent with the discussion above indicating that bulk  $\text{PM}_{2.5}$  pH is higher due to the contributions of sea salt aerosol components solely in the 1 to 2.5  $\mu\text{m}$  range. For smaller particles ( $\text{PM}_1$ ), these components don’t significantly affect the  $\text{SO}_4^{2-}$ - $\text{NO}_3^-$ - $\text{NH}_4^+$ - $\text{HNO}_3$ - $\text{NH}_3$  system resulting in a lower bulk  $\text{PM}_1$  pH. Size resolved particle pH and solubility of metals, reported in another study, are consistent with these findings (Fang et al., 2017). (Note, an attempt to calculate pH in the  $\text{PM}_1$  to  $\text{PM}_{2.5}$  size range was not successful due to highly uncertain data resulting from particle concentrations determined by difference from two separate measurements).

## 25 4. Discussion

### 4.1 Cause for bias in $\varepsilon(\text{NO}_3^-)$

The bias between ISORROPIA-predicted and observed nitrate partitioning may be a result of several causes. Since the  $\varepsilon(\text{NO}_3^-)$  bias is seen for both  $\text{PM}_1$  (AMS-data) and  $\text{PM}_{2.5}$  (PILS-IC data), the cause is apparently not associated with a specific aerosol measurement method. For the aerosol measurements, sampling artifacts associated with differences in indoor-outdoor temperatures that varied with time of day could be one cause for the biases. Sample heating is most likely to occur at night (indoor T > ambient T) and can cause semi-volatile  $\text{NO}_3^-$  loss, whereas sample cooling during the day (indoor

T < ambient T) can lead to vapor condensation and higher  $\text{NO}_3^-$ . Differences in observed versus predicted  $\text{NO}_3^-$  are consistent with these trends (Fig. S5); measured  $\text{NO}_3^-$  is lower than predicted at night (negative artifact) and higher than predicted during the day (positive artifact). The same will apply to  $\text{NH}_3\text{-NH}_4^+$  partitioning, but to a lesser degree due to the addition of non-volatile sulfate. Indoor temperatures were recorded to be fairly constant at  $\sim 25^\circ\text{C}$  for the AMS trailer (Fig. S6, PILS trailer indoor temperatures are expected to be similar). Aerosol samples were heated by  $\sim 10^\circ\text{C}$  at night and negligibly during the middle of the day (Table S1). Possible biases due to effects of the altered RH and T on aerosol measurements were examined by comparing measurements to model results for partitioning of  $\text{HNO}_3\text{-NO}_3^-$ ,  $\text{NH}_3\text{-NH}_4^+$  using sample line versus ambient conditions (Figs. S6 and S7), with all other model inputs the same. We find that ambient RH and T result in better agreement for  $\text{NO}_3^-$ ,  $\epsilon(\text{NO}_3^-)$ ,  $\text{NH}_4^+$ ,  $\epsilon(\text{NH}_4^+)$ , although some minor effect may be possible. We note that more extreme ambient to sample line temperature differences were experienced during the WINTER aircraft campaign ( $\Delta T$  on average  $+24^\circ\text{C}$ ). In that case, a similar analysis also found no evidence for nitrate loss due to sample line heating (Guo et al., 2016). (Sample-line residence times of 0.5 to 2 seconds are in a same range for both studies).

The sampling systems for  $\text{HNO}_3$  and  $\text{NH}_3$  involved heated sample inlets, which could also lead to bias due to evaporation of aerosol components. Here we only focus on the CIMS sampling line heating ( $75^\circ\text{C}$ ) since it was more extreme than the  $\text{NH}_3$  ( $40^\circ\text{C}$ ). For the CIMS system, a  $75^\circ\text{C}$  inlet may cause particle nitrate and chloride evaporation (residence time = 0.32 sec, Table S1), resulting in over-measurement of  $\text{HNO}_3$  and  $\text{HCl}$  (the species measured by this instrument). To examine whether this is the cause for the differences in predicted and observed  $\epsilon(\text{NO}_3^-)$ , we compared the partitioning of  $\text{HNO}_3\text{-NO}_3^-$ ,  $\text{NH}_3\text{-NH}_4^+$  based on “corrected”  $\text{HNO}_3$  assuming 10%, 20% and 30% of the measured  $\text{NO}_3^-$  evaporated in the CIMS inlet (the “corrected”  $\text{HNO}_3$  is lower by subtracting the various fractions of  $\text{PM}_{10} \text{NO}_3^-$  from measured  $\text{HNO}_3$ ). Comparing the orthogonal regression fitting lines in the Fig. S8, only slight improvements in predicted to measured  $\epsilon(\text{NO}_3^-)$  are found for increased  $\text{NO}_3^-$  loss (Fig. S8c), but all lines converge at the same intercept. At 30% evaporation the comparison becomes worse for both  $\epsilon(\text{NO}_3^-)$  and  $\epsilon(\text{NH}_4^+)$ . We conclude that potential inlet artifacts associated with the aerosol or gas phase sampling systems cannot explain the predicted versus measured  $\epsilon(\text{NO}_3^-)$  bias. This is consistent with the limited inlet heating and residence times in this study compared to some thermodenuder studies utilizing more extreme conditions (Huffman et al., 2009; Riipinen et al., 2010).

Another possible cause of the  $\epsilon(\text{NO}_3^-)$  bias is the effect of a large sea salt coarse mode on fine mode semi-volatile species. For example, during nighttime when  $\text{HNO}_3$  concentrations are much lower relative to daytime, ISORROPIA-II may have overestimated  $\text{NO}_3^-$  due to ignoring the presence of a larger more neutral coarse mode when calculating fine mode aerosol concentrations assuming equilibrium. Various studies show the typical time for the fine mode to reach thermodynamic equilibrium is on the order of 20 minutes (Dassios and Pandis, 1999; Fountoukis et al., 2009), whereas time scales for the coarse mode to equilibrate are much larger. The mixing of fine particles with high concentrations of coarse mode, mainly sea salt, particles could disrupt fine mode equilibrium by the mass transfer of volatile fine mode  $\text{NO}_3^-$ , via  $\text{HNO}_3$ , to the coarse mode, forming non-volatile salts, such as  $\text{NaNO}_3$ . This mechanism is consistent with the presence of high levels of sea salt in the LA region and the anti-correlation of a  $\text{NO}_3^-$  prediction bias with  $\text{HNO}_3$  concentration (Fig. S5). During the daytime,

when  $\text{HNO}_3$  concentrations are high, this bias would be minimal, but at night when  $\text{HNO}_3$  concentrations are low, the model, which ignores the presence of the coarse mode, would over-predict  $\text{NO}_3^-$  concentrations, by not considering fine mode nitrate loss to the coarse mode. Again, partitioning of  $\text{NH}_3$ - $\text{NH}_4^+$  would not be affected as much by this process since some fraction of the  $\text{NH}_4^+$  would be associated with  $\text{SO}_4^{2-}$ . Of the various locations where we have investigated pH, this study has the highest coarse mode inorganic aerosol concentrations (Sardar et al. (2005) reports levels of  $\sim 20 \mu\text{g m}^{-3}$  year round) and is the only one where we have observed this bias (not observed in the eastern US reported by Guo et al. (2016)).

#### 4.2 Why is nitrate much higher in LA compared to other regions investigated?

A comparison of pH and related statistics in five field studies is summarized in Table 2. The campaigns are CalNex, SOAS, SENEX, and WINTER, all conducted in the continental US. Also included are results from a study in the eastern Mediterranean (the campaign acronyms are given in Table 2). The SOAS (ground-based) and SENEX (aircraft-based) studies provide an interesting contrast with CalNex; that is between the southeastern versus southwestern US in summertime. WINTER aircraft data adds the dimension of seasonal variation (summer versus winter). The eastern Mediterranean data provides a remote European (Crete) and urban (Athens) perspective, and a case where air masses were known to be impacted by biomass burning (BB). All pH in Table 2 were calculated by ISORROPIA-II in forward metastable mode, but only the US data (SOAS, WINTER, CalNex) used gas-particle phase partitioning to constrain and verify the pH prediction for all the data analyzed. Lack of  $\text{NH}_3$  or  $\text{HNO}_3$  data for the eastern Mediterranean means that pH was likely underestimated by  $\sim 0.5$  units (Bougiatioti et al., 2016b). This was verified with a limited set of data when both aerosol and gas-phase data was available. It is noteworthy that in all studies, pH was low and on average below 3. The eastern US regions are characterized with the lowest pH ( $\sim 1$ ) throughout the year, from ground level up to 5 km aloft (Guo et al., 2015; Guo et al., 2016; Xu et al., 2016). The highest pH of  $2.8 \pm 0.6$  was consistently observed in biomass burning impacted air masses, regardless of season in both the remote and urban eastern Mediterranean and attributed to an abundance of  $\text{NH}_3$  and fine particle  $\text{K}^+$  in biomass burning emissions, which raised pH and  $\text{NO}_3^-$  concentrations significantly (Bougiatioti et al., 2016a). Biomass burning also accounted for the high pH, which approaches 3, in Athens during winter.

Comparing LA (CalNex) to the other summertime measurements in the eastern US (SOAS, SENEX), Table 2 shows that the LA ground site had uniquely higher  $\text{NO}_3^-$  and  $\text{HNO}_3$  mass concentrations and  $\text{NO}_3^-$  was the most abundant (by mass) inorganic ion for  $\text{PM}_1$  or  $\text{PM}_{2.5}$ . In contrast, in the southeastern US in summertime,  $\text{SO}_4^{2-}$  was the dominant ion,  $\text{NO}_3^-$  was only 5-14% of the  $\text{SO}_4^{2-}$  mass. The higher total  $\text{NO}_3^-$  ( $\text{NO}_3^- + \text{HNO}_3$ ) in LA indicates high local  $\text{NO}_x$  relative to  $\text{SO}_2$  sources. LA also had roughly 1 unit higher  $\text{PM}_1$  pH, and much higher  $\text{NO}_3^-$  concentrations relative to  $\text{SO}_4^{2-}$ . (Total ammonia ( $\text{NH}_3 + \text{NH}_4^+$ ) was also higher (Table 2)). The ratio of total  $\text{NO}_3^-$  and  $\text{SO}_4^{2-}$  (sulfate is non-volatile so total sulfate is equivalent to sulfate) was  $\sim 4$  for CalNex, compared to 0.3 for SOAS and 0.8 for SENEX. The higher ratio of total  $\text{NO}_3^-$  to  $\text{SO}_4^{2-}$  can explain the higher LA pH through coupling of particle composition, hygroscopicity, and acidity. Consider the situation where there is initially a high  $\text{HNO}_3$  concentration. Some  $\text{HNO}_3$  will condense onto very acidic particles (e.g., even at low

$\epsilon(\text{NO}_3^-)$ , with very high  $\text{HNO}_3$ , some  $\text{NO}_3^-$  can form). If this  $\text{NO}_3^-$  is significant relative to  $\text{SO}_4^{2-}$ , it substantially increases the particle  $W_i$ , which dilutes the  $\text{H}^+$  and raises the pH, since  $\text{NO}_3^-$  has a similarly high hygroscopicity as  $\text{SO}_4^{2-}$  (Nenes et al., 1998). Higher pH leads to more  $\text{NO}_3^-$  formed. This positive feedback, which reaches equilibrium at some point, and along with the condition of higher abundance of  $\text{NH}_3$  compared to the southeast (Table 2), may explain the higher  $\text{NO}_3^-$  and one unit higher pH in LA. This feedback process only happens for semi-volatile highly hygroscopic species. Sulfate will not have this effect since it is non-volatile. It also can only happen when the semi-volatile species contributes a large fraction to the particle  $W_i$ , hence high total  $\text{NO}_3^-$  to  $\text{SO}_4^{2-}$  ratios, which is why the effect is not seen in the eastern US in summertime. To better understand the relationship between  $\text{NO}_3^-$ , pH and T across different campaigns, S curves calculated from solubility and dissociation of a species in water, with activity coefficients included, provide a useful conceptual means for comparing pH predictions from the thermodynamic model to measurements of semi-volatile species partitioning between gas-particle phases (see Fig. 5). The inter-comparison between the various campaigns is shown in Figure 8. For each campaign, data are selected within a narrow range (see Figure 8 caption) to limit the effects of  $W_i$  and T variations on gas-particle partitioning. (CalNex  $\text{PM}_{2.5}$  pH is not included in Figure 8 due to very limited points since CalNex  $\text{PM}_{2.5}$   $W_i$  was much higher due to high inorganic mass loadings and an average RH of 87%). S curves are calculated based on a  $W_i$  of  $2.5 \mu\text{gm}^{-3}$  and T of 0 and 20 °C for wintertime or summertime conditions, respectively. ISORROPIA-II predicted activity coefficient of the  $\text{H}^+ \text{--} \text{NO}_3^-$  ion pair,  $\gamma_{\text{H}^+ \text{--} \text{NO}_3^-}$ , is included to account for aqueous solution non-ideality.

Consider the nitrate partitioning case,  $\epsilon(\text{NO}_3^-)$ , comparing SOAS to WINTER (Fig. 8a versus 8b). Although the data pH ranges are similar in these studies (on average  $\sim 1$ ), there is higher  $\epsilon(\text{NO}_3^-)$  in winter (T = 0 °C) due to the S curve shifting to lower pH ( $\sim 1$  unit) relative to summer (T = 20 °C), illustrating the effect of T (which is mainly through  $\text{HNO}_3$  Henry's law constant sensitivity to T). Considering only Fig 8b; as noted above, the temperature ranges were more similar for the SOAS, SENEX and Calnex studies, yet CalNex had higher particle pH ( $\text{PM}_{10}$ ) and more nitrate compared to SOAS and SENEX due to higher total  $\text{NO}_3$  relative to  $\text{SO}_4^{2-}$ , which leads to more nitrate formation through feed backs involving particle water and pH, as discussed above. This can also be seen in Fig 8b.

$\epsilon(\text{NH}_4^+)$  S curves and data from the field studies are shown in Fig. 8c and 8d. Note that the  $\epsilon(\text{NO}_3^-)$  and  $\epsilon(\text{NH}_4^+)$  face opposite directions since acid versus base.  $\text{NH}_3$  data was not available during WINTER so no measured  $\epsilon(\text{NH}_4^+)$  points were plotted at 0°C and no comparisons as a function of T can be made. At 20°C, the  $\epsilon(\text{NH}_4^+)$  of CalNex, SOAS, and SENEX all converge around one S curve, which was calculated assuming  $\gamma_{\text{H}^+ \text{--} \text{NH}_4^+}=1$ . The lower pH of SOAS and SENEX relative to CalNex resulted in generally higher  $\epsilon(\text{NH}_4^+)$ , more ammonia partitioned to the particle phase. The data and predicted  $\epsilon(\text{NH}_4^+)$  are in fairly good agreement.

S curves have significant utility for understanding how T, RH and pH affect partitioning (e.g., see Fig. S3&S4), but we also note that they can be used to estimate activity coefficients based on partitioning data, which may be particularly useful in situations where the data is not available from literature (e.g., organic acids above a mixture of inorganic and organics).

## 5. Summary

pH of PM<sub>1</sub> and PM<sub>2.5</sub>, and the semi-volatile gas-particle partitioning of HNO<sub>3</sub>-NO<sub>3</sub><sup>-</sup>, NH<sub>3</sub>-NH<sub>4</sub><sup>+</sup> and HCl-Cl<sup>-</sup> in the Los Angeles basin during the 2010 CalNex study were investigated. As a coastal urban site impacted by high sea salt aerosol components, and high total nitrate (HNO<sub>3</sub>+NO<sub>3</sub><sup>-</sup>), and ammonia levels, this study provided a contrast to pH we have reported in the eastern US and eastern Mediterranean.

PM<sub>1</sub> single particle analysis showed that 73% (by number) of PM<sub>1</sub> sea salt particles did not contain nitrate and sea salt type particles only contributed to 12% to PM<sub>1</sub> mass. Therefore, PM<sub>1</sub> pH was predicted solely on the SO<sub>4</sub><sup>2-</sup>-NO<sub>3</sub><sup>-</sup>-NH<sub>4</sub><sup>+</sup>-HNO<sub>3</sub>-NH<sub>3</sub> system (ISORROPIA-II inputs). This approach provided good agreement between observed and model-predicted partitioning of NH<sub>3</sub>-NH<sub>4</sub><sup>+</sup> and HNO<sub>3</sub>-NO<sub>3</sub><sup>-</sup>, although a bias in  $\epsilon(\text{NO}_3^-)$  was observed that depended on RH (day vs. night). Altering gas and particle temperatures from ambient due to the sampling configurations did not explain the bias. A likely cause is the loss of fine mode NO<sub>3</sub><sup>-</sup> to coarse mode sea salt, mainly at night when HNO<sub>3</sub> concentrations are low, which is not considered by the thermodynamic model used to predict fine mode concentrations.

The study mean ( $\pm$  SD) PM<sub>1</sub> pH in the LA basin was  $1.9 \pm 0.5$ , roughly one unit higher than the average pH observed in summer in the southeastern US ( $0.9 \pm 0.6$  and  $1.1 \pm 0.4$ ), despite similar RH and T ranges and both calculated for the SO<sub>4</sub><sup>2-</sup>-NO<sub>3</sub><sup>-</sup>-NH<sub>4</sub><sup>+</sup>-HNO<sub>3</sub>-NH<sub>3</sub> system. The cause may be much higher total nitrate concentrations (high NO<sub>x</sub> and proximity to locations of HNO<sub>3</sub> formation) relative to sulfate in LA. For example, high levels of HNO<sub>3</sub> can lead to at least some particulate NO<sub>3</sub><sup>-</sup>, even if conditions are such that NO<sub>3</sub><sup>-</sup> partitioning is low (e.g.,  $\epsilon(\text{NO}_3^-)$  is small). NO<sub>3</sub><sup>-</sup> increases the particle water, which raises pH by dilution of H<sup>+</sup>, allowing more partitioning (i.e., increases  $\epsilon(\text{NO}_3^-)$ ). When non-volatile sulfate dominates over total nitrate, sulfate controls liquid water and this effect is not observed. The complex interactions between pH, LWC, T, and NO<sub>3</sub><sup>-</sup> are clearly illustrated by analytical (“S” curve) analyses.

Single particle analysis showed that 85% by number of sea salt particles in the 1 to 2.5  $\mu\text{m}$  nominal range contained nitrate and that the model predicted partitioning of HNO<sub>3</sub>-NO<sub>3</sub><sup>-</sup> for PM<sub>2.5</sub> agreed better with the observed partitioning when sea salt components were included (SO<sub>4</sub><sup>2-</sup>-NO<sub>3</sub><sup>-</sup>-NH<sub>4</sub><sup>+</sup>-Na<sup>+</sup>-Cl<sup>-</sup>-K<sup>+</sup>-HNO<sub>3</sub>-NH<sub>3</sub>-HCl system). Bulk PM<sub>2.5</sub> pH was  $2.7 \pm 0.3$ , whereas for the same time period PM<sub>1</sub> pH was  $1.9 \pm 0.4$  and the diurnal pH profiles of PM<sub>1</sub> and PM<sub>2.5</sub> also differed, all apparently due to the influence of sea salt aerosols.

The CalNex data provides unique contrast to pH reported in other regions and demonstrates the complex interactions between pH and emissions. It also supports the general application of SO<sub>4</sub><sup>2-</sup>-NO<sub>3</sub><sup>-</sup>-NH<sub>4</sub><sup>+</sup>-HNO<sub>3</sub>-NH<sub>3</sub> system for predictions of PM<sub>1</sub> pH and gas-particle phase partitioning without considering sea salts or crustal elements, useful for regional or global modeling. It further illustrates that fine particles have surprisingly low pH in many locations, which has significant effects on the many environmental impacts of fine particles.

**Acknowledgements.** Georgia Tech researchers were funded through National Science Foundation (NSF) grants AGS-0931492 and AGS-0802237. This work was also supported by NSF under grants AGS-1242258 and AGS-1360730 that

supported our participation in the SOAS and WINTER campaigns. We wish to thank Aikaterini Bougiatioti for sharing the eastern Mediterranean data included in Table 2 and Raluca Ellis and Jennifer Murphy for use of the gas phase ammonia data. PLH and JLJ were partially supported by NSF AGS-1360834. We thank Amber Ortega for providing the residence time in the AMS inlet. The NOAA work was supported by the NOAA Air Quality and Climate Research programs.

5

## Reference

- Ansari, A. S., and Pandis, S. N.: The effect of metastable equilibrium states on the partitioning of nitrate between the gas and aerosol phases, *Atmospheric Environment*, 34, 157-168, doi: 10.1016/s1352-2310(99)00242-3, 2000.
- 10 Bertram, A. K., Martin, S. T., Hanna, S. J., Smith, M. L., Bodsworth, A., Chen, Q., Kuwata, M., Liu, A., You, Y., and Zorn, S. R.: Predicting the relative humidities of liquid-liquid phase separation, efflorescence, and deliquescence of mixed particles of ammonium sulfate, organic material, and water using the organic-to-sulfate mass ratio of the particle and the oxygen-to-carbon elemental ratio of the organic component, *Atmospheric Chemistry and Physics*, 11, 10995-11006, doi: 10.5194/acp-11-10995-2011, 2011.
- 15 Bougiatioti, A., Nenes, A., Paraskevopoulou, D., Fountziou, L., Stavroulas, I., Liakakou, E., Weber, R., Gerasopoulou, E., Nikolaou, P., and Mihalopoulos, N.: The unappreciated effects of biomass burning on fine mode aerosol acidity, water and nitrogen partitioning, In review, 2016a.
- Bougiatioti, A., Nikolaou, P., Stavroulas, I., Kouvarakis, G., Weber, R., Nenes, A., Kanakidou, M., and Mihalopoulos, N.: Particle water and pH in the Eastern Mediterranean: Sources variability and implications for  
20 nutrients availability, *Atmospheric Chemistry and Physics*, 16, 4579-4591, doi: 10.5194/acp-16-4579-2016, 2016b.
- Carlsaw, K. S., Clegg, S. L., and Brimblecombe, P.: A Thermodynamic Model of the System HCl-HNO<sub>3</sub>-H<sub>2</sub>SO<sub>4</sub>-H<sub>2</sub>O, Including Solubilities of Hbr, from <200 to 328 K, *Journal of Physical Chemistry*, 99, 11557-11574, doi: 10.1021/j100029a039, 1995.
- 25 Clegg, S. L., and Brimblecombe, P.: Equilibrium Partial Pressures and Mean Activity and Osmotic Coefficients of 0-100-Percent Nitric-Acid as a Function of Temperature, *Journal of Physical Chemistry*, 94, 5369-5380, doi: 10.1021/j100376a038, 1990.
- Clegg, S. L., Brimblecombe, P., and Wexler, A. S.: Thermodynamic model of the system H<sup>+</sup>-NH<sub>4</sub><sup>+</sup>-SO<sub>4</sub><sup>2-</sup>-NO<sub>3</sub><sup>-</sup>-H<sub>2</sub>O at tropospheric temperatures, *J Phys Chem A*, 102, 2137-2154, doi: 10.1021/Jp973042r, 1998.
- 30 Clegg, S. L., Seinfeld, J. H., and Edney, E. O.: Thermodynamic modelling of aqueous aerosols containing electrolytes and dissolved organic compounds. II. An extended Zdanovskii–Stokes–Robinson approach, *Journal of Aerosol Science*, 34, 667-690, doi: 10.1016/s0021-8502(03)00019-3, 2003.
- Dassios, K. G., and Pandis, S. N.: The mass accommodation coefficient of ammonium nitrate aerosol, *Atmospheric Environment*, 33, 2993-3003, doi: 10.1016/S1352-2310(99)00079-5, 1999.
- 35 DeCarlo, P. F., Kimmel, J. R., Trimborn, A., Northway, M. J., Jayne, J. T., Aiken, A. C., Gonin, M., Fuhrer, K., Horvath, T., Docherty, K. S., Worsnop, D. R., and Jimenez, J. L.: Field-deployable, high-resolution, time-of-flight aerosol mass spectrometer, *Analytical chemistry*, 78, 8281-8289, doi: 10.1021/ac061249n, 2006.
- Dockery, D. W., Cunningham, J., Damokosh, A. I., Neas, L. M., Spengler, J. D., Koutrakis, P., Ware, J. H., Raizenne, M., and Speizer, F. E.: Health effects of acid aerosols on North American children: respiratory  
40 symptoms, *Environ Health Perspect*, 104, 500-505, 1996.

- Duce, R. A., and Tindale, N. W.: Atmospheric transport of iron and its deposition in the ocean, *Limnol Oceanogr*, 36, 1715-1726, doi: 10.4319/lo.1991.36.8.1715, 1991.
- Duyzer, J.: Dry deposition of ammonia and ammonium aerosols over heathland, *J Geophys Res-Atmos*, 99, 18757-18763, doi: Doi 10.1029/94jd01210, 1994.
- 5 Eddingsaas, N. C., VanderVelde, D. G., and Wennberg, P. O.: Kinetics and Products of the Acid-Catalyzed Ring-Opening of Atmospherically Relevant Butyl Epoxy Alcohols, *J Phys Chem A*, 114, 8106-8113, doi: 10.1021/Jp103907c, 2010.
- Edney, E. O., Kleindienst, T. E., Jaoui, M., Lewandowski, M., Offenberg, J. H., Wang, W., and Claeys, M.: Formation of 2-methyl tetrols and 2-methylglyceric acid in secondary organic aerosol from laboratory  
10 irradiated isoprene/NO<sub>x</sub>/SO<sub>2</sub>/air mixtures and their detection in ambient PM<sub>2.5</sub> samples collected in the eastern United States, *Atmospheric Environment*, 39, 5281-5289, doi: 10.1016/j.atmosenv.2005.05.031, 2005.
- Ellis, R. A., Murphy, J. G., Pattey, E., van Haarlem, R., O'Brien, J. M., and Herndon, S. C.: Characterizing a Quantum Cascade Tunable Infrared Laser Differential Absorption Spectrometer (QC-TILDAS) for measurements of atmospheric ammonia, *Atmospheric Measurement Techniques*, 3, 397-406, doi: 10.5194/amt-3-397-2010, 2010.
- 15 Enami, S., Hoffmann, M. R., and Colussi, A. J.: Acidity enhances the formation of a persistent ozonide at aqueous ascorbate/ozone gas interfaces, *Proceedings of the National Academy of Sciences of the United States of America*, 105, 7365-7369, doi: 10.1073/pnas.0710791105, 2008.
- Fang, T., Guo, H., Verma, V., Peltier, R. E., and Weber, R. J.: PM<sub>2.5</sub> water-soluble elements in the southeastern  
20 United States: automated analytical method development, spatiotemporal distributions, source apportionment, and implications for health studies, *Atmospheric Chemistry and Physics*, 15, 11667-11682, doi: 10.5194/acp-15-11667-2015, 2015.
- Fang, T., Guo, H., Zeng, L., Verma, V., Nenes, A., and Weber, R. J.: Highly acidic ambient particles, soluble metals and oxidative potential: A link between sulfate and aerosol toxicity, *Environmental science & technology*, doi: 10.1021/acs.est.6b06151, 2017.
- 25 Fountoukis, C., and Nenes, A.: ISORROPIA II: a computationally efficient thermodynamic equilibrium model for K<sup>+</sup>-Ca<sup>2+</sup>-Mg<sup>2+</sup>-NH<sub>4</sub><sup>+</sup>-Na<sup>+</sup>-SO<sub>4</sub><sup>2-</sup>-NO<sub>3</sub><sup>-</sup>-Cl<sup>-</sup>-H<sub>2</sub>O aerosols, *Atmospheric Chemistry and Physics*, 7, 4639-4659, doi: 10.5194/acp-7-4639-2007, 2007.
- Fountoukis, C., Nenes, A., Sullivan, A., Weber, R., Van Reken, T., Fischer, M., Matias, E., Moya, M., Farmer, D., and Cohen, R. C.: Thermodynamic characterization of Mexico City aerosol during MILAGRO 2006, *Atmospheric Chemistry and Physics*, 9, 2141-2156, doi: 10.5194/acp-9-2141-2009, 2009.
- 30 Froyd, K. D., Murphy, D. M., Lawson, P., Baumgardner, D., and Herman, R. L.: Aerosols that form subvisible cirrus at the tropical tropopause, *Atmospheric Chemistry and Physics*, 10, 209-218, doi: 10.5194/acp-10-209-2010, 2010.
- 35 Gao, S., Keywood, M., Ng, N. L., Surratt, J., Varutbangkul, V., Bahreini, R., Flagan, R. C., and Seinfeld, J. H.: Low-molecular-weight and oligomeric components in secondary organic aerosol from the ozonolysis of cycloalkenes and α-pinene, *J Phys Chem A*, 108, 10147-10164, doi: 10.1021/Jp047466e, 2004.
- Ghio, A. J., Carraway, M. S., and Madden, M. C.: Composition of air pollution particles and oxidative stress in cells, tissues, and living systems, *Journal of toxicology and environmental health. Part B, Critical reviews*, 15, 1-21, doi: 10.1080/10937404.2012.632359, 2012.
- 40 Guo, H., Xu, L., Bougiatioti, A., Cerully, K. M., Capps, S. L., Hite, J. R., Carlton, A. G., Lee, S. H., Bergin, M. H., Ng, N. L., Nenes, A., and Weber, R. J.: Fine-particle water and pH in the southeastern United States, *Atmospheric Chemistry and Physics*, 15, 5211-5228, doi: 10.5194/acp-15-5211-2015, 2015.
- Guo, H., Sullivan, A. P., Campuzano-Jost, P., Schroder, J. C., Lopez-Hilfiker, F. D., Dibb, J. E., Jimenez, J. L., Thornton, J. A., Brown, S. S., Nenes, A., and Weber, R. J.: Fine particle pH and the partitioning of nitric acid
- 45



- during winter in the northeastern United States, *Journal of Geophysical Research: Atmospheres*, 121, 10,355-310,376, doi: 10.1002/2016jd025311, 2016.
- Gwynn, R. C., Burnett, R. T., and Thurston, G. D.: A time-series analysis of acidic particulate matter and daily mortality and morbidity in the Buffalo, New York, region, *Environ Health Perspect*, 108, 125-133, 2000.
- 5 Han, Y., Stroud, C. A., Liggo, J., and Li, S.-M.: The effect of particle acidity on secondary organic aerosol formation from  $\alpha$ -pinene photooxidation under atmospherically relevant conditions, *Atmospheric Chemistry and Physics Discussions*, 1-26, doi: 10.5194/acp-2016-301, 2016.
- Hand, J. L., Schichtel, B. A., Pitchford, M., Malm, W. C., and Frank, N. H.: Seasonal composition of remote and urban fine particulate matter in the United States, *Journal of Geophysical Research: Atmospheres*, 117, D05209, doi: 10.1029/2011jd017122, 2012.
- 10 Hayes, P. L., Ortega, A. M., Cubison, M. J., Froyd, K. D., Zhao, Y., Cliff, S. S., Hu, W. W., Toohey, D. W., Flynn, J. H., Lefer, B. L., Grossberg, N., Alvarez, S., Rappenglück, B., Taylor, J. W., Allan, J. D., Holloway, J. S., Gilman, J. B., Kuster, W. C., de Gouw, J. A., Massoli, P., Zhang, X., Liu, J., Weber, R. J., Corrigan, A. L., Russell, L. M., Isaacman, G., Worton, D. R., Kreisberg, N. M., Goldstein, A. H., Thalman, R., Waxman, E. M., Volkamer, R., Lin, Y. H., Surratt, J. D., Kleindienst, T. E., Offenberg, J. H., Dusanter, S., Griffith, S., Stevens, P. S., Brioude, J., Angevine, W. M., and Jimenez, J. L.: Organic aerosol composition and sources in Pasadena, California, during the 2010 CalNex campaign, *Journal of Geophysical Research: Atmospheres*, 118, 9233-9257, doi: 10.1002/jgrd.50530, 2013.
- 15 Hayes, P. L., Carlton, A. G., Baker, K. R., Ahmadov, R., Washenfelder, R. A., Alvarez, S., Rappenglück, B., Gilman, J. B., Kuster, W. C., de Gouw, J. A., Zotter, P., Prévôt, A. S. H., Szidat, S., Kleindienst, T. E., Offenberg, J. H., Ma, P. K., and Jimenez, J. L.: Modeling the formation and aging of secondary organic aerosols in Los Angeles during CalNex 2010, *Atmospheric Chemistry and Physics*, 15, 5773-5801, doi: 10.5194/acp-15-5773-2015, 2015.
- 20 Hennigan, C. J., Sandholm, S., Kim, S., Stickel, R. E., Huey, L. G., and Weber, R. J.: Influence of Ohio River valley emissions on fine particle sulfate measured from aircraft over large regions of the eastern United States and Canada during INTEX-NA, *J Geophys Res-Atmos*, 111, doi: 10.1029/2006/Jd007282, 2006.
- 25 Hennigan, C. J., Sullivan, A. P., Fountoukis, C. I., Nenes, A., Hecobian, A., Vargas, O., Peltier, R. E., Hanks, A. T. C., Huey, L. G., Lefer, B. L., Russell, A. G., and Weber, R. J.: On the volatility and production mechanisms of newly formed nitrate and water soluble organic aerosol in Mexico City, *Atmospheric Chemistry and Physics*, 8, 3761-3768, 2008.
- 30 Hennigan, C. J., Izumi, J., Sullivan, A. P., Weber, R. J., and Nenes, A.: A critical evaluation of proxy methods used to estimate the acidity of atmospheric particles, *Atmospheric Chemistry and Physics*, 15, 2775-2790, doi: 10.5194/acp-15-2775-2015, 2015.
- Huebert, B. J., and Robert, C. H.: The Dry Deposition of Nitric-Acid to Grass, *J Geophys Res-Atmos*, 90, 2085-2090, doi: 10.1029/JD090iD01p02085, 1985.
- 35 Huffman, J. A., Docherty, K. S., Aiken, A. C., Cubison, M. J., Ulbrich, I. M., DeCarlo, P. F., Sueper, D., Jayne, J. T., Worsnop, D. R., Ziemann, P. J., and Jimenez, J. L.: Chemically-resolved aerosol volatility measurements from two megacity field studies, *Atmospheric Chemistry and Physics*, 9, 7161-7182, doi: 10.5194/acp-9-7161-2009, 2009.
- 40 IPCC: Climate Change 2013: The Physical Science Basis. Working Group I Contribution to the Fifth Assessment Report of the International Panel on Climate Change., Cambridge, United Kingdom and New York, NY, USA, 1535, 2013.
- Ito, A., and Xu, L.: Response of acid mobilization of iron-containing mineral dust to improvement of air quality projected in the future, *Atmospheric Chemistry and Physics*, 14, 3441-3459, doi: 10.5194/acp-14-3441-2014, 45 2014.

- Ito, T., Nenes, A., Johnson, M. S., Meskhidze, N., and Deutsch, C.: Acceleration of oxygen decline in the tropical Pacific over the past decades by aerosol pollutants, *Nature Geoscience*, 9, 443-447, doi: 10.1038/ngeo2717, 2016.
- Jang, M., Czoschke, N. M., Lee, S., and Kamens, R. M.: Heterogeneous atmospheric aerosol production by acid-catalyzed particle-phase reactions, *Science*, 298, 814-817, doi: 10.1126/science.1075798, 2002.
- Koutrakis, P., Wolfson, J. M., and Spengler, J. D.: An improved method for measuring aerosol strong acidity: Results from a nine-month study in St Louis, Missouri and Kingston, Tennessee, *Atmospheric Environment* (1967), 22, 157-162, doi: 10.1016/0004-6981(88)90308-3, 1988.
- Langer, S., Pemberton, R. S., and Finlayson-Pitts, B. J.: Diffuse Reflectance Infrared Studies of the Reaction of Synthetic Sea Salt Mixtures with NO<sub>2</sub>: A Key Role for Hydrates in the Kinetics and Mechanism, *The Journal of Physical Chemistry A*, 101, 1277-1286, doi: 10.1021/jp962122c, 1997.
- Last, J. A.: Global atmospheric change: potential health effects of acid aerosol and oxidant gas mixtures, *Environ Health Perspect*, 96, 151-157, doi: 10.1289/ehp.9196151, 1991.
- Lelieveld, J., Evans, J. S., Fnais, M., Giannadaki, D., and Pozzer, A.: The contribution of outdoor air pollution sources to premature mortality on a global scale, *Nature*, 525, 367-371, doi: 10.1038/nature15371, 2015.
- Li, W., Xu, L., Liu, X., Zhang, J., Lin, Y., Yao, X., Gao, H., Zhang, D., Chen, J., Wang, W., Harrison, R., Zhang, X., Shao, L., Fu, P., Nenes, A., and Shi, Z.: Air pollution - aerosol interactions produce more bioavailable iron for ocean ecosystems, *Sci. Advance*, In press.
- Lim, S. S., Vos, T., Flaxman, A. D., Danaei, G., Shibuya, K., Adair-Rohani, H., AlMazroa, M. A., Amann, M., Anderson, H. R., Andrews, K. G., Aryee, M., Atkinson, C., Bacchus, L. J., Bahalim, A. N., Balakrishnan, K., Balmes, J., Barker-Collo, S., Baxter, A., Bell, M. L., Blore, J. D., Blyth, F., Bonner, C., Borges, G., Bourne, R., Boussinesq, M., Brauer, M., Brooks, P., Bruce, N. G., Brunekreef, B., Bryan-Hancock, C., Bucello, C., Buchbinder, R., Bull, F., Burnett, R. T., Byers, T. E., Calabria, B., Carapetis, J., Carnahan, E., Chafe, Z., Charlson, F., Chen, H., Chen, J. S., Cheng, A. T.-A., Child, J. C., Cohen, A., Colson, K. E., Cowie, B. C., Darby, S., Darling, S., Davis, A., Degenhardt, L., Dentener, F., Des Jarlais, D. C., Devries, K., Dherani, M., Ding, E. L., Dorsey, E. R., Driscoll, T., Edmond, K., Ali, S. E., Engell, R. E., Erwin, P. J., Fahimi, S., Falder, G., Farzadfar, F., Ferrari, A., Finucane, M. M., Flaxman, S., Fowkes, F. G. R., Freedman, G., Freeman, M. K., Gakidou, E., Ghosh, S., Giovannucci, E., Gmel, G., Graham, K., Grainger, R., Grant, B., Gunnell, D., Gutierrez, H. R., Hall, W., Hoek, H. W., Hogan, A., Hosgood Iii, H. D., Hoy, D., Hu, H., Hubbell, B. J., Hutchings, S. J., Ibeanusi, S. E., Jacklyn, G. L., Jasrasaria, R., Jonas, J. B., Kan, H., Kanis, J. A., Kassebaum, N., Kawakami, N., Khang, Y.-H., Khatibzadeh, S., Khoo, J.-P., Kok, C., Laden, F., Lalloo, R., Lan, Q., Lathlean, T., Leasher, J. L., Leigh, J., Li, Y., Lin, J. K., Lipshultz, S. E., London, S., Lozano, R., Lu, Y., Mak, J., Malekzadeh, R., Mallinger, L., Marcenes, W., March, L., Marks, R., Martin, R., McGale, P., McGrath, J., Mehta, S., Memish, Z. A., Mensah, G. A., Merriman, T. R., Micha, R., Michaud, C., Mishra, V., Hanafiah, K. M., Mokdad, A. A., Morawska, L., Mozaffarian, D., Murphy, T., Naghavi, M., Neal, B., Nelson, P. K., Nolla, J. M., Norman, R., Olives, C., Omer, S. B., Orchard, J., Osborne, R., Ostro, B., Page, A., Pandey, K. D., Parry, C. D. H., Passmore, E., Patra, J., Pearce, N., Pelizzari, P. M., Petzold, M., Phillips, M. R., Pope, D., Pope Iii, C. A., Powles, J., Rao, M., Razavi, H., Rehfuss, E. A., Rehm, J. T., Ritz, B., Rivara, F. P., Roberts, T., Robinson, C., Rodriguez-Portales, J. A., Romieu, I., Room, R., Rosenfeld, L. C., Roy, A., Rushton, L., Salomon, J. A., Sampson, U., Sanchez-Riera, L., Sanman, E., Sapkota, A., Seedat, S., Shi, P., Shield, K., Shivakoti, R., Singh, G. M., Sleet, D. A., Smith, E., Smith, K. R., Stapelberg, N. J. C., Steenland, K., Stöckl, H., Stovner, L. J., Straif, K., Straney, L., Thurston, G. D., Tran, J. H., Van Dingenen, R., van Donkelaar, A., Veerman, J. L., Vijayakumar, L., Weintraub, R., Weissman, M. M., White, R. A., Whiteford, H., Wiersma, S. T., Wilkinson, J. D., Williams, H. C., Williams, W., Wilson, N., Woolf, A. D., Yip, P., Zielinski, J. M., Lopez, A. D., Murray, C. J. L., and Ezzati, M.: A comparative risk assessment of burden of disease and injury attributable to 67 risk factors and risk factor clusters in 21 regions, 1990–2010: a systematic analysis for the Global Burden of

- Disease Study 2010, *The Lancet*, 380, 2224-2260, doi: [http://dx.doi.org/10.1016/S0140-6736\(12\)61766-8](http://dx.doi.org/10.1016/S0140-6736(12)61766-8), 2012.
- Liu, J., Zhang, X., Parker, E. T., Veres, P. R., Roberts, J. M., de Gouw, J. A., Hayes, P. L., Jimenez, J. L., Murphy, J. G., Ellis, R. A., Huey, L. G., and Weber, R. J.: On the gas-particle partitioning of soluble organic aerosol in two urban atmospheres with contrasting emissions: 2. Gas and particle phase formic acid, *Journal of Geophysical Research*, 117, D00V21, doi: 10.1029/2012jd017912, 2012.
- Longo, A. F., Feng, Y., Lai, B., Landing, W. M., Shelley, R. U., Nenes, A., Mihalopoulos, N., Violaki, K., and Ingall, E. D.: Influence of Atmospheric Processes on the Solubility and Composition of Iron in Saharan Dust, *Environmental science & technology*, 50, 6912-6920, doi: 10.1021/acs.est.6b02605, 2016.
- 10 Malm, W. C., and Day, D. E.: Estimates of aerosol species scattering characteristics as a function of relative humidity, *Atmospheric Environment*, 35, 2845-2860, doi: 10.1016/S1352-2310(01)00077-2, 2001.
- Mei, F., Hayes, P. L., Ortega, A., Taylor, J. W., Allan, J. D., Gilman, J., Kuster, W., de Gouw, J., Jimenez, J. L., and Wang, J.: Droplet activation properties of organic aerosols observed at an urban site during CalNex-LA, *Journal of Geophysical Research: Atmospheres*, 118, 2903-2917, doi: 10.1002/jgrd.50285, 2013.
- 15 Meskhidze, N., Chameides, W. L., Nenes, A., and Chen, G.: Iron mobilization in mineral dust: Can anthropogenic SO<sub>2</sub> emissions affect ocean productivity?, *Geophysical Research Letters*, 30, 2085, doi: 10.1029/2003gl018035, 2003.
- Middlebrook, A. M., Bahreini, R., Jimenez, J. L., and Canagaratna, M. R.: Evaluation of Composition-Dependent Collection Efficiencies for the Aerodyne Aerosol Mass Spectrometer using Field Data, *Aerosol Science and Technology*, 46, 258-271, doi: 10.1080/02786826.2011.620041, 2012.
- 20 Murphy, D. M., Cziczo, D. J., Froyd, K. D., Hudson, P. K., Matthew, B. M., Middlebrook, A. M., Peltier, R. E., Sullivan, A., Thomson, D. S., and Weber, R. J.: Single-particle mass spectrometry of tropospheric aerosol particles, *Journal of Geophysical Research*, 111, doi: 10.1029/2006jd007340, 2006.
- Myriokefalitakis, S., Daskalakis, N., Mihalopoulos, N., Baker, A. R., Nenes, A., and Kanakidou, M.: Changes in dissolved iron deposition to the oceans driven by human activity: a 3-D global modelling study, *Biogeosciences*, 12, 3973-3992, doi: 10.5194/bg-12-3973-2015, 2015.
- 25 Nenes, A., Pandis, S. N., and Pilinis, C.: ISORROPIA: A new thermodynamic equilibrium model for multiphase multicomponent inorganic aerosols, *Aquat Geochem*, 4, 123-152, doi: 10.1023/A:1009604003981, 1998.
- Nenes, A., Krom, M. D., Mihalopoulos, N., Van Cappellen, P., Shi, Z., Bougiatioti, A., Zampas, P., and Herut, B.: Atmospheric acidification of mineral aerosols: a source of bioavailable phosphorus for the oceans, *Atmospheric Chemistry and Physics*, 11, 6265-6272, doi: 10.5194/acp-11-6265-2011, 2011.
- 30 Oakes, M., Ingall, E. D., Lai, B., Shafer, M. M., Hays, M. D., Liu, Z. G., Russell, A. G., and Weber, R. J.: Iron solubility related to particle sulfur content in source emission and ambient fine particles, *Environmental science & technology*, 46, 6637-6644, doi: 10.1021/es300701c, 2012.
- 35 Orsini, D. A., Ma, Y., Sullivan, A., Sierau, B., Baumann, K., and Weber, R. J.: Refinements to the particle-into-liquid sampler (PILS) for ground and airborne measurements of water soluble aerosol composition, *Atmospheric Environment*, 37, 1243-1259, doi: 10.1016/s1352-2310(02)01015-4, 2003.
- Peltier, R. E., Sullivan, A. P., Weber, R. J., Brock, C. A., Wollny, A. G., Holloway, J. S., de Gouw, J. A., and Warneke, C.: Fine aerosol bulk composition measured on WP-3D research aircraft in vicinity of the Northeastern United States - results from NEAQS, *Atmospheric Chemistry and Physics*, 7, 3231-3247, doi: 10.5194/acp-7-3231-2007, 2007.
- 40 Raizenne, M., Neas, L. M., Damokosh, A. I., Dockery, D. W., Spengler, J. D., Koutrakis, P., Ware, J. H., and Speizer, F. E.: Health effects of acid aerosols on North American children: pulmonary function, *Environ Health Perspect*, 104, 506-514, 1996.

- Riipinen, I., Pierce, J. R., Donahue, N. M., and Pandis, S. N.: Equilibration time scales of organic aerosol inside thermodenuders: Evaporation kinetics versus thermodynamics, *Atmospheric Environment*, 44, 597-607, doi: 10.1016/j.atmosenv.2009.11.022, 2010.
- Robbins, R. C., Cadle, R. D., and Eckhardt, D. L.: The Conversion of Sodium Chloride to Hydrogen Chloride in the Atmosphere, *Journal of Meteorology*, 16, 53-56, doi: 10.1175/1520-0469(1959)016<0053:tcosct>2.0.co;2, 1959.
- Ryerson, T. B., Andrews, A. E., Angevine, W. M., Bates, T. S., Brock, C. A., Cairns, B., Cohen, R. C., Cooper, O. R., de Gouw, J. A., Fehsenfeld, F. C., Ferrare, R. A., Fischer, M. L., Flagan, R. C., Goldstein, A. H., Hair, J. W., Hardesty, R. M., Hostetler, C. A., Jimenez, J. L., Langford, A. O., McCauley, E., McKeen, S. A., Molina, L. T., Nenes, A., Oltmans, S. J., Parrish, D. D., Pederson, J. R., Pierce, R. B., Prather, K., Quinn, P. K., Seinfeld, J. H., Senff, C. J., Sorooshian, A., Stutz, J., Surratt, J. D., Trainer, M., Volkamer, R., Williams, E. J., and Wofsy, S. C.: The 2010 California Research at the Nexus of Air Quality and Climate Change (CalNex) field study, *Journal of Geophysical Research: Atmospheres*, 118, 5830-5866, doi: 10.1002/jgrd.50331, 2013.
- Sardar, S. B., Fine, P. M., and Sioutas, C.: Seasonal and spatial variability of the size-resolved chemical composition of particulate matter (PM<sub>10</sub>) in the Los Angeles Basin, *J Geophys Res-Atmos*, 110, D07S08, doi: 10.1029/2004jd004627, 2005.
- Schill, G. P., and Tolbert, M. A.: Heterogeneous ice nucleation on phase-separated organic-sulfate particles: effect of liquid vs. glassy coatings, *Atmospheric Chemistry and Physics*, 13, 4681-4695, doi: 10.5194/acp-13-4681-2013, 2013.
- Schrader, F., and Brummer, C.: Land Use Specific Ammonia Deposition Velocities: a Review of Recent Studies (2004-2013), *Water, air, and soil pollution*, 225, 2114, doi: 10.1007/s11270-014-2114-7, 2014.
- Song, M., Marcolli, C., Krieger, U. K., Zuend, A., and Peter, T.: Liquid-liquid phase separation and morphology of internally mixed dicarboxylic acids/ammonium sulfate/water particles, *Atmospheric Chemistry and Physics*, 12, 2691-2712, doi: 10.5194/acp-12-2691-2012, 2012.
- Sullivan, A. P., Peltier, R. E., Brock, C. A., de Gouw, J. A., Holloway, J. S., Warneke, C., Wollny, A. G., and Weber, R. J.: Airborne measurements of carbonaceous aerosol soluble in water over northeastern United States: Method development and an investigation into water-soluble organic carbon sources, *Journal of Geophysical Research*, 111, D23S46, doi: 10.1029/2006jd007072, 2006.
- Surratt, J. D., Lewandowski, M., Offenberg, J. H., Jaoui, M., Kleindienst, T. E., Edney, E. O., and Seinfeld, J. H.: Effect of acidity on secondary organic aerosol formation from isoprene, *Environmental science & technology*, 41, 5363-5369, doi: 10.1021/es0704176, 2007.
- Surratt, J. D., Chan, A. W., Eddingsaas, N. C., Chan, M., Loza, C. L., Kwan, A. J., Hersey, S. P., Flagan, R. C., Wennberg, P. O., and Seinfeld, J. H.: Reactive intermediates revealed in secondary organic aerosol formation from isoprene, *Proceedings of the National Academy of Sciences of the United States of America*, 107, 6640-6645, doi: 10.1073/pnas.0911114107, 2010.
- Thurston, G. D., Ito, K., Hayes, C. G., Bates, D. V., and Lippmann, M.: Respiratory hospital admissions and summertime haze air pollution in Toronto, Ontario: consideration of the role of acid aerosols, *Environ Res*, 65, 271-290, doi: 10.1006/enrs.1994.1037, 1994.
- Veres, P., Roberts, J. M., Warneke, C., Welsh-Bon, D., Zahniser, M., Herndon, S., Fall, R., and de Gouw, J.: Development of negative-ion proton-transfer chemical-ionization mass spectrometry (NI-PT-CIMS) for the measurement of gas-phase organic acids in the atmosphere, *International Journal of Mass Spectrometry*, 274, 48-55, doi: 10.1016/j.ijms.2008.04.032, 2008.
- Veres, P. R., Roberts, J. M., Cochran, A. K., Gilman, J. B., Kuster, W. C., Holloway, J. S., Graus, M., Flynn, J., Lefer, B., Warneke, C., and de Gouw, J.: Evidence of rapid production of organic acids in an urban air mass, *Geophysical Research Letters*, 38, L17807, doi: 10.1029/2011gl048420, 2011.

- Verma, V., Fang, T., Guo, H., King, L., Bates, J. T., Peltier, R. E., Edgerton, E., Russell, A. G., and Weber, R. J.: Reactive oxygen species associated with water-soluble PM<sub>2.5</sub> in the southeastern United States: spatiotemporal trends and source apportionment, *Atmospheric Chemistry and Physics*, 14, 12915-12930, doi: 10.5194/acp-14-12915-2014, 2014.
- 5 Washenfelder, R. A., Young, C. J., Brown, S. S., Angevine, W. M., Atlas, E. L., Blake, D. R., Bon, D. M., Cubison, M. J., de Gouw, J. A., Dusanter, S., Flynn, J., Gilman, J. B., Graus, M., Griffith, S., Grossberg, N., Hayes, P. L., Jimenez, J. L., Kuster, W. C., Lefer, B. L., Pollack, I. B., Ryerson, T. B., Stark, H., Stevens, P. S., and Trainer, M. K.: The glyoxal budget and its contribution to organic aerosol for Los Angeles, California, during CalNex 2010, *Journal of Geophysical Research: Atmospheres*, 116, doi: 10.1029/2011jd016314, 2011.
- 10 Weber, R. J., Guo, H., Russell, A. G., and Nenes, A.: High aerosol acidity despite declining atmospheric sulfate concentrations over the past 15 years, *Nature Geoscience*, 9, 282-285, doi: 10.1038/ngeo2665, 2016.
- Wexler, A. S., and Clegg, S. L.: Atmospheric aerosol models for systems including the ions H<sup>+</sup>, NH<sub>4</sub><sup>+</sup>, Na<sup>+</sup>, SO<sub>4</sub><sup>2-</sup>, NO<sub>3</sub><sup>-</sup>, Cl<sup>-</sup>, Br<sup>-</sup>, and H<sub>2</sub>O, *Journal of Geophysical Research*, 107, 4207, doi: 10.1029/2001jd000451, 2002.
- 15 Xu, L., Middlebrook, A. M., Liao, J., de Gouw, J. A., Guo, H., Weber, R. J., Nenes, A., Lopez-Hilfiker, F. D., Lee, B. H., Thornton, J. A., Brock, C. A., Neuman, J. A., Nowak, J. B., Pollack, I. B., Welti, A., Graus, M., Warneke, C., and Ng, N. L.: Enhanced formation of isoprene-derived organic aerosol in sulfur-rich power plant plumes during Southeast Nexus, *Journal of Geophysical Research: Atmospheres*, 121, 11,137-111,153, doi: 10.1002/2016jd025156, 2016.
- 20 Ye, Q., Robinson, E. S., Ding, X., Ye, P., Sullivan, R. C., and Donahue, N. M.: Mixing of secondary organic aerosols versus relative humidity, *Proceedings of the National Academy of Sciences of the United States of America*, doi: 10.1073/pnas.1604536113, 2016.
- You, Y., Renbaum-Wolff, L., and Bertram, A. K.: Liquid–liquid phase separation in particles containing organics mixed with ammonium sulfate, ammonium bisulfate, ammonium nitrate or sodium chloride, *Atmospheric Chemistry and Physics*, 13, 11723-11734, doi: 10.5194/acp-13-11723-2013, 2013.
- 25 You, Y., Smith, M. L., Song, M., Martin, S. T., and Bertram, A. K.: Liquid–liquid phase separation in atmospherically relevant particles consisting of organic species and inorganic salts, *International Reviews in Physical Chemistry*, 33, 43-77, doi: 10.1080/0144235x.2014.890786, 2014.
- You, Y., and Bertram, A. K.: Effects of molecular weight and temperature on liquid–liquid phase separation in particles containing organic species and inorganic salts, *Atmospheric Chemistry and Physics*, 15, 1351-1365, doi: 10.5194/acp-15-1351-2015, 2015.
- 30 Zhang, Q., Jimenez, J. L., Canagaratna, M. R., Allan, J. D., Coe, H., Ulbrich, I., Alfarra, M. R., Takami, A., Middlebrook, A. M., Sun, Y. L., Dzepina, K., Dunlea, E., Docherty, K., DeCarlo, P. F., Salcedo, D., Onasch, T., Jayne, J. T., Miyoshi, T., Shimonono, A., Hatakeyama, S., Takegawa, N., Kondo, Y., Schneider, J., Drewnick, F., Borrmann, S., Weimer, S., Demerjian, K., Williams, P., Bower, K., Bahreini, R., Cottrell, L., Griffin, R. J., Rautiainen, J., Sun, J. Y., Zhang, Y. M., and Worsnop, D. R.: Ubiquity and dominance of oxygenated species in organic aerosols in anthropogenically-influenced Northern Hemisphere midlatitudes, *Geophysical Research Letters*, 34, L13801, doi: 10.1029/2007gl029979, 2007.
- 35

**Table 1.** Number fraction of sea salt particles with observable nitrate signals and mass fraction of sea salt particles to total mass in two size ranges, 0.15-1 and 1-2.5  $\mu\text{m}$ . Sea salt particles are identified as  $\text{Na}^+$ -rich particles without crustal elements. The number fraction was determined directly from the PALMS data and the mass fraction was calculated based on the number fractions and size distributions, assuming dry particle densities.

Particle size, $\mu\text{m}$	Number fraction of sea salt particles with observable nitrate signal	Sea salt particles mass fraction to total
0.15-1	27%	12%
1-2.5	85%	63%

5

**Table 2.** Comparisons between different studies for particle pH, major inorganic ions and gases and meteorological conditions. All pH values are from ISORROPIA-II run in forward-mode. The campaign acronyms other than CalNex stand for Southern Oxidant and Aerosol Study (SOAS), Southeastern Nexus of Air Quality and Climate (SENEX), Wintertime Investigation of Transport, Emissions, and Reactivity (WINTER).

Campaign	CalNex		SOAS	SENEX <sup>c</sup>	WINTER	Studies in the eastern Mediterranean		
Type	Ground	Ground	Ground	Aircraft	Aircraft	Ground	Ground	(BB plumes) <sup>f</sup>
PM cut size	PM <sub>1</sub>	PM <sub>2.5</sub> <sup>a</sup>	PM <sub>1</sub> &PM <sub>2.5</sub> <sup>b</sup>	PM <sub>1</sub>	PM <sub>1</sub>	PM <sub>1</sub>	PM <sub>1</sub>	PM <sub>1</sub>
Year	2010		2013	2013	2015	2012	2013-2014	2012-2014
Season	(Early) Summer		Summer	Summer	Winter	Summer-Autumn	Winter	Summer-Winter
Region/Location	SW US		SE US	SE US	NE US	Crete, Greece	Athens, Greece	Crete&Athens
SO <sub>4</sub> <sup>2-</sup> , µg m <sup>-3</sup>	2.86 ± 1.70	1.88 ± 0.69	1.73 ± 1.21	2.05 ± 0.80	1.02 ± 0.77	2.31 ± 1.61	2.31 ± 1.32	1.66 ± 1.49
NO <sub>3</sub> <sup>-</sup> , µg m <sup>-3</sup>	3.58 ± 3.65	3.74 ± 1.53	0.08 ± 0.08	0.28 ± 0.09	0.80 ± 1.03	0.12 ± 0.07	2.21 ± 2.02	1.79 ± 1.49
HNO <sub>3</sub> , µg m <sup>-3</sup>	6.65 ± 7.03	4.45 ± 3.59	0.36 ± 0.14	1.35 ± 0.66	1.41 ± 1.83	\	\	0.91 ± 0.39
ε(NO <sub>3</sub> <sup>-</sup> )	39 ± 16%	51 ± 18%	22 ± 16%	18 ± 6%	37 ± 28%	< 20% <sup>e</sup>	\	65 ± 14%
Total NO <sub>3</sub> <sup>-</sup> , µg m <sup>-3</sup>	10.22 ± 9.74	8.19 ± 3.89	0.45 ± 0.26	1.63 ± 0.70	2.21 ± 2.21	\	\	3.36 ± 2.08
NH <sub>4</sub> <sup>+</sup> , µg m <sup>-3</sup>	2.06 ± 1.67	1.79 ± 0.65	0.46 ± 0.34	1.06 ± 0.25	0.50 ± 0.43	0.81 ± 0.58	1.96 ± 1.30	1.02 ± 0.93
NH <sub>3</sub> , µg m <sup>-3</sup>	1.37 ± 0.90	0.75 ± 0.61	0.39 ± 0.25	0.12 ± 0.19	\	\	\	\
ε(NH <sub>4</sub> <sup>+</sup> )	55 ± 25%	71 ± 19%	50 ± 25%	92 ± 11%	\	\	\	\
Total NH <sub>4</sub> <sup>+</sup> , µg m <sup>-3</sup>	3.44 ± 1.81	2.54 ± 0.89	0.78 ± 0.50	1.17 ± 0.81	\	\	\	\
Na <sup>+</sup> , µg m <sup>-3</sup>	\	0.77 ± 0.39	0.03 ± 0.07	\	0.23 ± 0.46 <sup>d</sup>	0.19 ± 0.43	0.13 ± 0.11	0.08 ± 0.05
Cl <sup>-</sup> , µg m <sup>-3</sup>	\	0.64 ± 0.48	0.02 ± 0.03	\	0.34 ± 0.38 <sup>d</sup>	0.22 ± 0.53	0.14 ± 0.19	0.20 ± 0.19
RH, %	79 ± 17	87 ± 9	74 ± 16	72 ± 9	58 ± 19	57 ± 11	80 ± 9	68 ± 16
T, °C	18 ± 4	18 ± 3	25 ± 3	22 ± 3	0 ± 8	27 ± 3	12 ± 3	20 ± 9
pH	<b>1.9 ± 0.5</b>	<b>2.7 ± 0.3</b>	<b>0.9 ± 0.6</b>	<b>1.1 ± 0.4</b>	<b>0.8 ± 1.0</b>	<b>1.3 ± 1.1</b>	<b>2.4 ± 0.8</b>	<b>2.8 ± 0.6</b>
Reference	This study		(Guo et al., 2015)	(Xu et al., 2016)	(Guo et al., 2016)	(Bougiatioti et al., 2016)	(Bougiatioti et al., 2017)	(Bougiatioti et al., 2016; 2017)

- 5 <sup>a</sup> Only the last week of CalNex; <sup>b</sup> PM<sub>2.5</sub> was sampled in the 1<sup>st</sup> half and PM<sub>1</sub> sampled in the 2<sup>nd</sup> half of the study; various parameters were similar in both cases, crustal components were higher, but overall generally low so differences had minor effects, e.g., PM<sub>2.5</sub> Na<sup>+</sup> was 0.06 ± 0.09 and PM<sub>1</sub> Na<sup>+</sup> was 0.01 ± 0.01 µgm<sup>-3</sup>; <sup>c</sup> Only one flight (June 16 2013) statistic from the reference is shown; <sup>d</sup> Externally mixed, thus not included in pH calculation; <sup>e</sup> Estimated from offline measurement; <sup>f</sup> Averaged from identified biomass burning (BB) plumes from Crete and Athens studies due to the similar pH; K<sup>+</sup> was 0.36 ± 0.38 µgm<sup>-3</sup>;

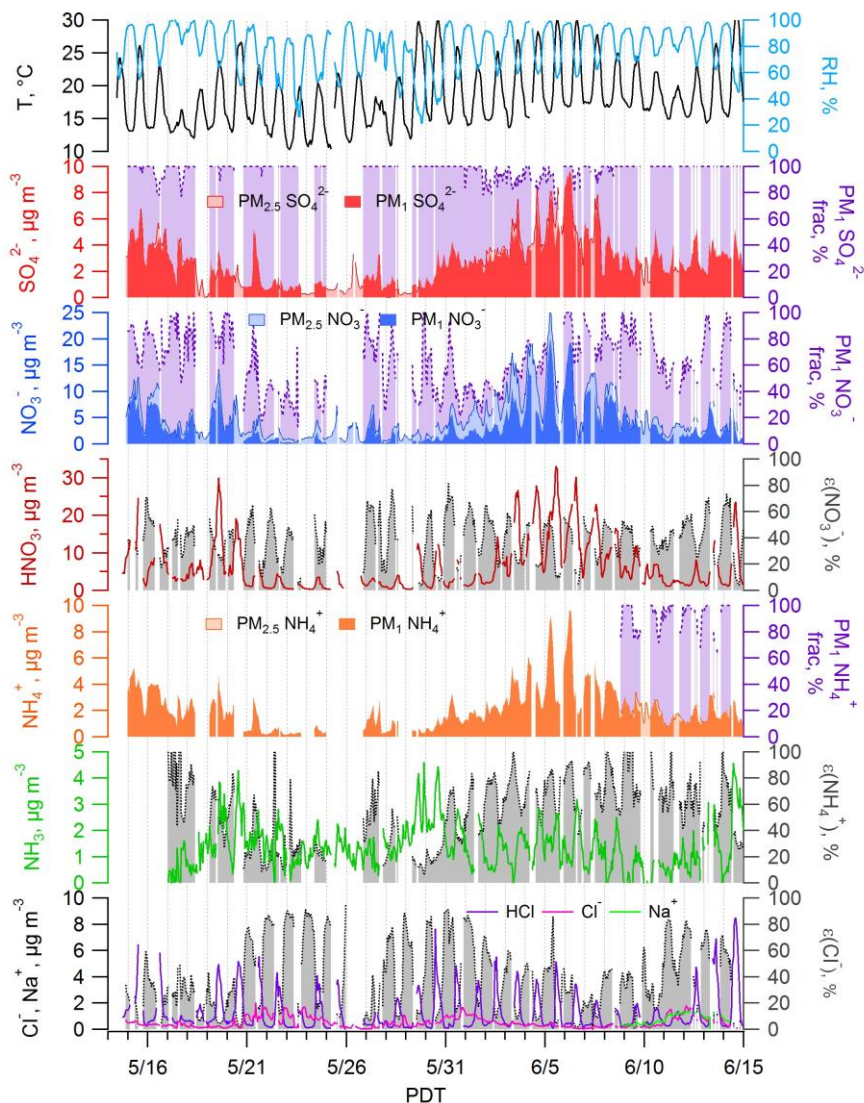


**Figure 1.** CalNex campaign time series of meteorological conditions (T, RH), particle- and gas-phase inorganic compound mass loadings ( $\text{SO}_4^{2-}$ ,  $\text{NO}_3^-$ ,  $\text{Cl}^-$ ,  $\text{NH}_4^+$ ,  $\text{Na}^+$ ;  $\text{HNO}_3$ ,  $\text{NH}_3$ ,  $\text{HCl}$ ), particle-phase mass fractions of total (gas plus particle;  $\epsilon(\text{NO}_3^-)$ ,  $\epsilon(\text{NH}_4^+)$  based on  $\text{PM}_{10}$  and  $\epsilon(\text{Cl}^-)$  based on  $\text{PM}_{2.5}$ , all denoted by grey color), and  $\text{PM}_{10}$  to  $\text{PM}_{2.5}$  mass fractions of  $\text{SO}_4^{2-}$ ,  $\text{NO}_3^-$ ,  $\text{NH}_4^+$  (all denoted by purple color).



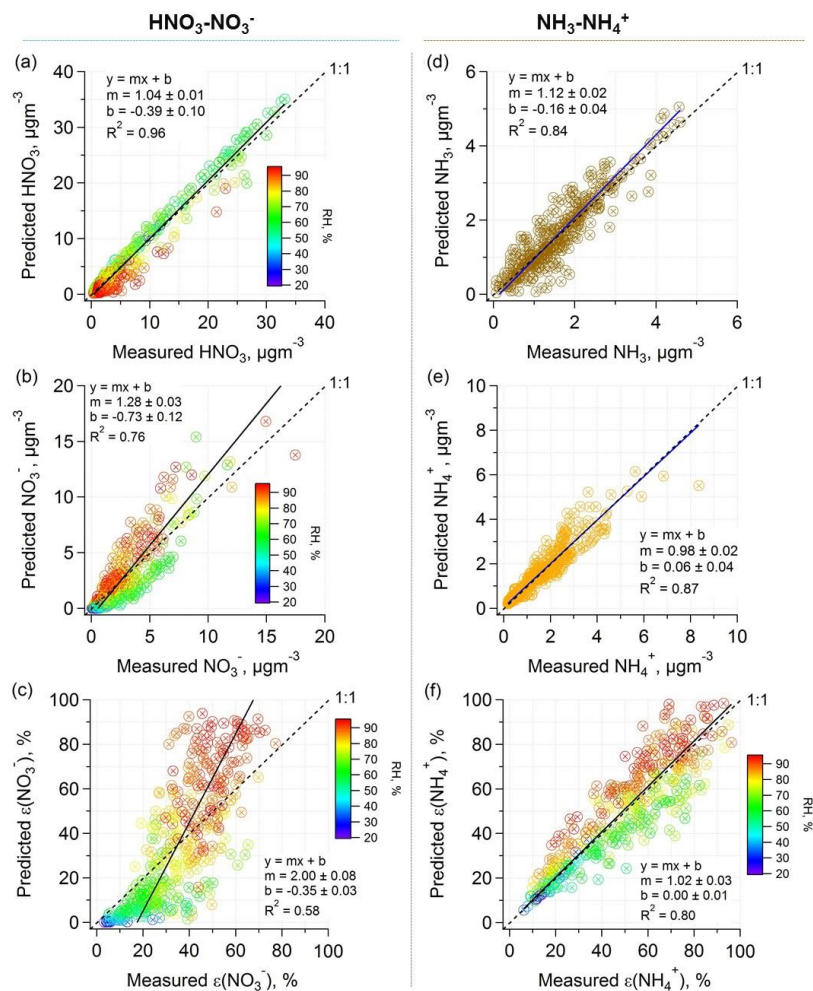


**Figure 2.** Comparisons of predicted and measured HNO<sub>3</sub>, NO<sub>3</sub><sup>-</sup>, and ε(NO<sub>3</sub><sup>-</sup>) (a, b, c) and NH<sub>3</sub>, NH<sub>4</sub><sup>+</sup>, and ε(NH<sub>4</sub><sup>+</sup>) (d, e, f) for data from the complete CalNex study. Particle-phase data are all AMS PM<sub>1</sub>. Orthogonal distance regression (ODR) fits are shown and uncertainties in the fits are one standard deviation.

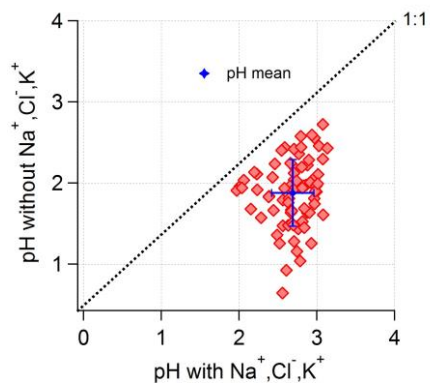


**Figure 3.** Comparison of predicted PM<sub>2.5</sub> particle pH assuming external versus internal mixing of Na<sup>+</sup>, Cl<sup>-</sup>, K<sup>+</sup> with SO<sub>4</sub><sup>2-</sup>, NO<sub>3</sub><sup>-</sup>, NH<sub>4</sub><sup>+</sup> for data from the last week of the CalNex study (i.e., SO<sub>4</sub><sup>2-</sup>-NO<sub>3</sub><sup>-</sup>-NH<sub>4</sub><sup>+</sup>-HNO<sub>3</sub>-NH<sub>3</sub> system vs. SO<sub>4</sub><sup>2-</sup>-NO<sub>3</sub><sup>-</sup>-NH<sub>4</sub><sup>+</sup>-Na<sup>+</sup>-Cl<sup>-</sup>-K<sup>+</sup>-HNO<sub>3</sub>-NH<sub>3</sub>-HCl system). For these two cases, pH increased from  $1.9 \pm 0.4$  to  $2.7 \pm 0.3$  with the input of Na<sup>+</sup>, Cl<sup>-</sup>, K<sup>+</sup>.

Figures 4 and 5 show that for PM<sub>2.5</sub>, inclusion of Na<sup>+</sup>, Cl<sup>-</sup>, K<sup>+</sup> provides better predicted portioning of nitric acid.

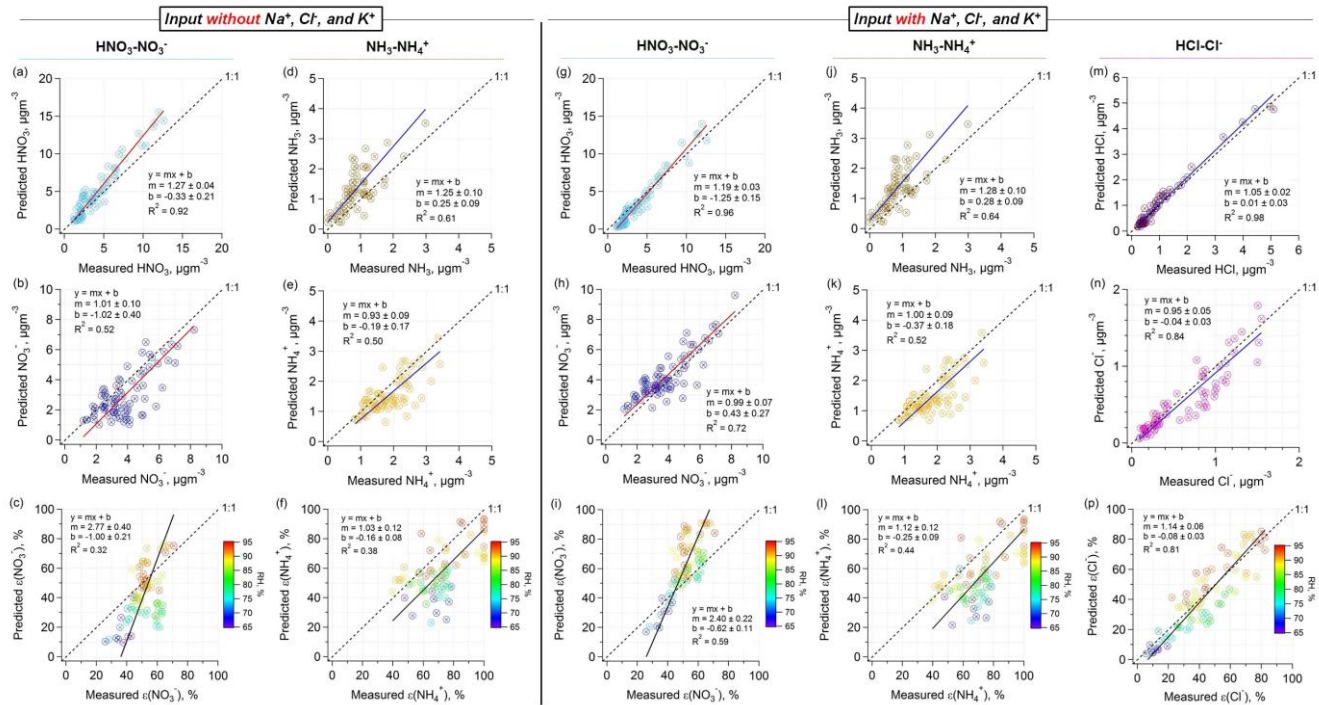


**Figure 4.** Inter-comparisons of predicted and measured gas-particle phase partitioning for  $\text{PM}_{2.5}$  particles for two scenarios: ISORROPIA-II input without (left) and with (right)  $\text{Na}^+$ ,  $\text{Cl}^-$  (and  $\text{HCl}$ ),  $\text{K}^+$ . The other input  $\text{SO}_4^{2-}$ ,  $\text{NO}_3^-$ ,  $\text{NH}_4^+$ ,  $\text{NH}_3$ ,  $\text{HNO}_3$ ,  $\text{RH}$ , and  $T$  are the same in the two cases. The  $\text{PM}_{2.5}$  data for the last week during CalNex study are shown above. ODR fits are applied.

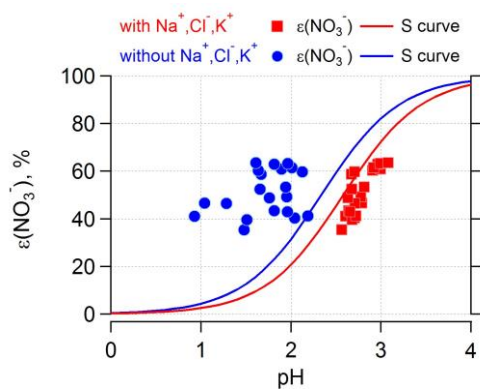


**Figure 5.** Comparison of measured  $\epsilon(\text{NO}_3^-)$  for  $\text{PM}_{2.5}$  (data points) to S curves, which are predicted from theory and include activity coefficients from ISORROPIA-II. The product of the activity coefficients,  $\gamma_{\text{H}^+}\gamma_{\text{NO}_3^-}$ , was on average 0.28 with  $\text{Na}^+$ ,  $\text{Cl}^-$ ,  $\text{K}^+$  and 0.19 without  $\text{Na}^+$ ,  $\text{Cl}^-$ ,  $\text{K}^+$ . In both cases pH (data points) is predicted by ISORROPIA-II.

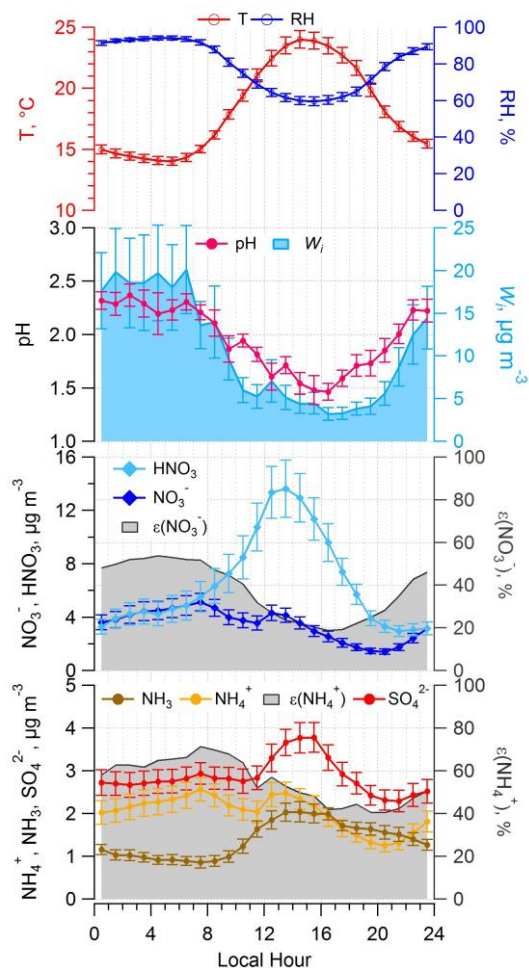


**Figure 6.** Diurnal profiles of predicted pH, LWC and measured T, RH, particle- and gas-phase inorganic compound mass loadings ( $\text{SO}_4^{2-}$ ,  $\text{NO}_3^-$ ,  $\text{NH}_4^+$ ,  $\text{HNO}_3$ ,  $\text{NH}_3$ ), and particle-phase fractions ( $\epsilon(\text{NO}_3^-)$ ,  $\epsilon(\text{NH}_4^+)$ ). Data shown above are for the complete CalNex campaign, and particle-phase data are AMS  $\text{PM}_{1.0}$ . Mean hourly averages are shown and standard errors are plotted as error bars.

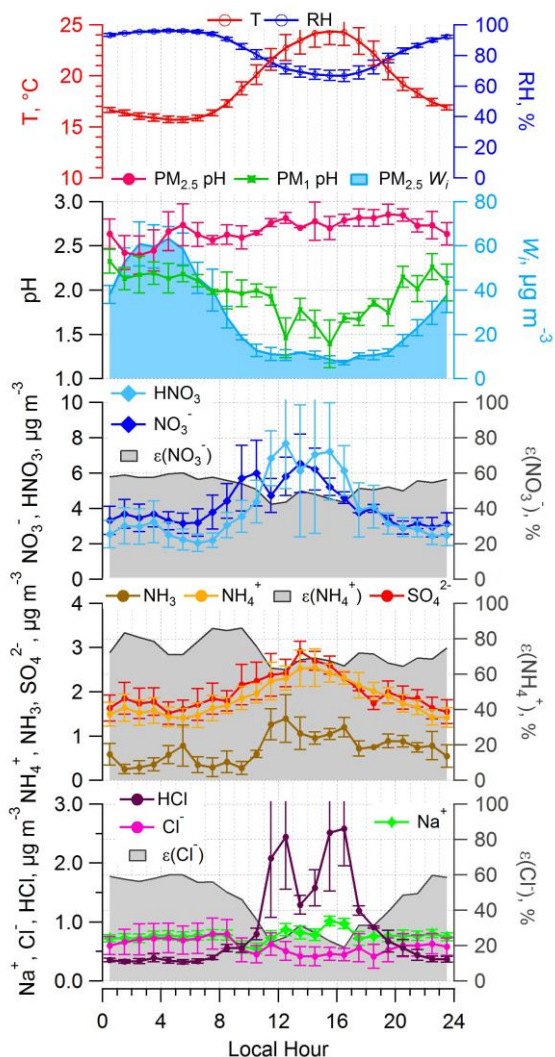


**Figure 7.** Diurnal profiles for the last week of CalNex of predicted pH and LWC, and measured T, RH, particle- and gas-phase inorganic compound mass loadings ( $\text{SO}_4^{2-}$ ,  $\text{NO}_3^-$ ,  $\text{Cl}^-$ ,  $\text{NH}_4^+$ ;  $\text{HNO}_3$ ,  $\text{NH}_3$ ,  $\text{HCl}$ ), particle-phase fractions ( $\epsilon(\text{NO}_3^-)$ ,  $\epsilon(\text{NH}_4^+)$ ,  $\epsilon(\text{Cl}^-)$ ). Particle-phase data are all PILS-IC  $\text{PM}_{2.5}$ . Median hourly averages are shown, and standard errors are plotted as error bars.

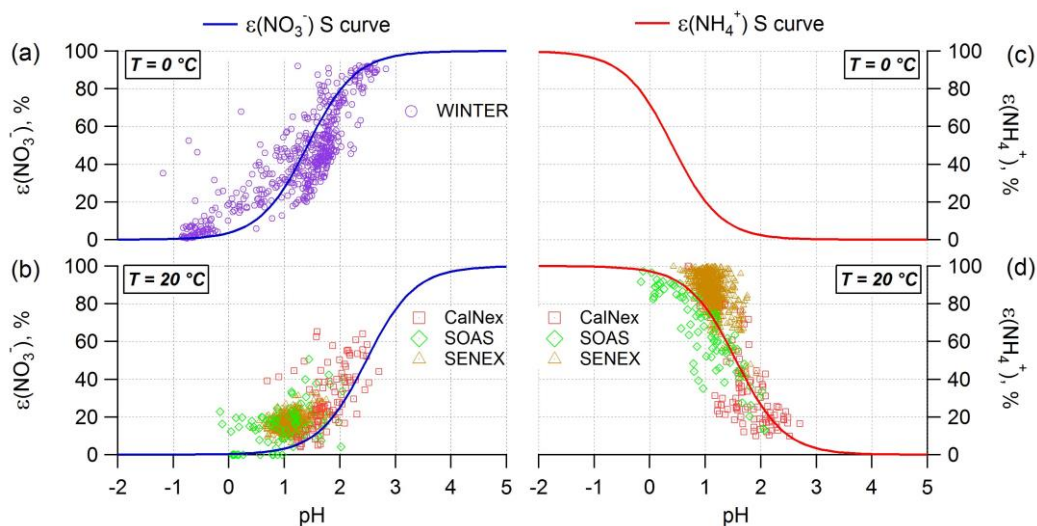


**Figure 8.** Analytically calculated S-curves of  $\epsilon(\text{NO}_3^-)$  and  $\epsilon(\text{NH}_4^+)$  and ambient data, plotted with ISORROPIA-predicted pH for CalNex, SOAS, SENEX, and WINTER studies.  $\epsilon(\text{NO}_3^-)$  and  $\epsilon(\text{NH}_4^+)$  are the fraction of the total (gas + particle) in the particle phase. For the data, a narrow range in  $W_i$  ( $1\text{--}4\ \mu\text{g m}^{-3}$ ) and  $T$  ( $-5 < T < 5^\circ\text{C}$  for  $T=0^\circ\text{C}$ ,  $15 < T < 25^\circ\text{C}$  for  $T=20^\circ\text{C}$ ) data were selected to be close to the analytical calculation input (i.e.,  $W_i = 2.5\ \mu\text{g m}^{-3}$  and various  $T$ ). For analytical calculations (S-curves),  $\gamma_{\text{NH}_4^+} = 1$  was applied; ISORROPIA-II predicted  $\gamma_{\text{H}^+ - \text{NO}_3^-}$  0.23 (WINTER) and 0.28 (CalNex 0.28, SOAS 0.29, SENEX 0.26) were used.